At the Interface of Isomorphous Behavior in a 3 x 3 Isomer Grid of Monochlorobenzamides: Analyses of the Interaction Landscapes via Contact Enrichment Studies

John Gallagher, Mark Farrell, Niall Hehir, Pavle Mocilac, Emmanuel Aubert, Enrique Espinosa, Benoît Guillot, Christian Jelsch

Published in *Crystal Growth & Design*, *19*(11), 6141-6158. doi.org/10.1021/acs.cgd.9b00505

At the interface of isomorphous behaviour in a 3×3 isomer grid of mono-chlorobenzamides: Analyses of the interaction landscapes *via* contact enrichment studies.

John F. Gallagher[*#], Mark Farrell, Niall Hehir, Pavle Mocilac,
School of Chemical Sciences, Dublin City University, Dublin 9, Ireland
and
Emmanuel Aubert, Enrique Espinosa, Benoît Guillot, Christian Jelsch[*]
CRM^2, CNRS UMR 7036, Faculté des Sciences et Technologies, Université de Lorraine,
BP 70239, Boulevard des Aiguillettes, 54506 Vandoeuvre-lès-Nancy, France

Abstract:
The physicochemical properties of a 3×3 isomer grid of mono-chlorobenzamides (**Clxx**) are reported with comprehensive studies of their crystal structures and interaction environments (**Clx** = *para*-/*meta*-/*ortho*-chlorobenzoyl and **x** = *para*-/*meta*-/*ortho*-aminopyridine substitutions). The nine compound **Clxx** series was synthesised from the three *p*-/*m*-/*o*-chlorobenzoyl chlorides and three *p*-/*m*-/*o*-aminopyridine isomers using standard synthetic procedures. **Clxx** exhibits some similarities to the related **Fxx** and **Brxx** congeners *e.g.* the isomorphous behaviour of **Clpp** (*para*-Chloro-*N*'-(*para*-pyridyl)benzamide) with several close relatives, and there are five isomorphous pairs of **Clxx** and **Brxx** crystal structures. Notably **Clmp** and **Clpm** both crystallise with *Z*'=4 in space group $P\bar{1}$ but show important differences. The overall lack of isomers crystallising with solvate molecules is noteworthy, except for **Clmm•**(H_2O). In all **Clxx** crystal structures, strong N-H…N hydrogen bonds form, however, **Clpo** also crystallises as the unexpected **Clpo_O** polymorph with N-H…O=C intermolecular hydrogen bonding. The **Clxo** triad (with *ortho*-pyridines) exhibits the expected cyclic N-H…N dimer formation with $R^2_2(8)$ hydrogen bonded rings. The H_C atom type, forming weak C-H…Cl hydrogen bonds, is the only favoured interaction partner of chlorine in **Clxx**. Conformational analyses (*gas phase*) together with crystal contact enrichment studies place **Clxx** in context and at the interface of hydrogen and halogen bonding interactions, though strong hydrogen bonding dominates. In **Clxx** the interaction energies with nearest neighbours are shown to contribute to most of the lattice electrostatic energies. The melting temperatures T_m show correlation with both molecular symmetry (Carnelley's rule) and total electrostatic energy of the weak interactions; in addition, these T_m values can be well predicted from a linear fit combining both descriptors. In **Clxx**, N-H…N hydrogen bonds dominate, largely in the absence of solvates, and with five **Clxx** forming isomorphous pairs with **Brxx** analogues; **Clpp** being isomorphous with several close benzamide relatives. Analysis of T_m reveals correlations involving both symmetry and electrostatic energies.

Keywords: Chlorine; Crystal structure; Conformational analysis; Contact Enrichments; Correlation; Electrostatic energy; Halogen; Melting Points; Pyridine.

Corresponding author:[#] Dr. John F. Gallagher, e-mail: john.gallagher@dcu.ie
School of Chemical Sciences, Dublin City University, Dublin 9, Ireland.

Introduction:

In the natural world, bromine and chlorine derivatives are pre-eminent amongst the >5000 known and naturally produced organo-halogen (***R*X**) compounds (where ***R*** = alkyl/aryl; **X** = halogen).[1-6] As such, naturally occurring fluorine and iodine compounds are much less common (at *ca*. 5% of the total). However, the recent and substantial rise in the use of fluorine in pharmaceuticals[7-8] and agrochemicals has been well documented.[9-12] The role and application of halogen atoms (and especially fluorine) in organic materials and pharmaceuticals has attracted widespread scientific interest.[13-19] The net effect of halogens on the chemical and physical properties of molecules and ultimately on research applications is an on-going scientific focus.[1-19] The key differences between the F, Cl, Br and I halogens are best exemplified in their respective steric and electronic properties. How these impact on and modify steric properties and electronic molecular environments is important. While fluorine is usually classified separately to chlorine, the heavier halogens bromine and iodine are often classified together in terms of their general chemical behaviour.[1-6,13-19] As such, organochlorine derivatives are generally studied as a distinct class and their behaviour and applications are readily contrasted with related organohalogens.[1-19]

The control and manipulation of intermolecular interactions lies at the heart of understanding molecular aggregation and therefore plays a central role in design and applications across supramolecular chemistry, crystal engineering and structural sciences.[20-24] Intra- and intermolecular interactions can play a role in influencing molecules towards the most favoured conformation(s) that are mostly retained in the crystal structure,[25-30] but unusual geometries can be stabilised in the crystal state. The whole range of interactions typically observed in organic molecules ranges from strong hydrogen bonding *e.g*. N/O-H…O/N, through moderate hydrogen/halogen bonding[31-39] through to C-H…π, aromatic donor-acceptor interactions to weaker contacts and van der Waals contacts.[25-30]

Halogen bonding, although recognised several decades ago has undergone an incredible surge in recent research activity.[31-39] While fluorine is often treated as a distinct entity, it is usually convenient to evaluate all of the halogens (F, Cl, Br I) to determine their steric and electronic influences on molecular structure and aggregation.[40-42] From a structural chemistry viewpoint, the role of chlorine in organic structures has not attracted the same attention as fluorine (fluoro-containing drugs) or the bromine/iodine pair (from a fundamental research perspective).[7,8,13-19,31-42] Despite this and given the major role of chlorinated compounds in the agricultural industry as insecticides and herbicides,[9-12] the present study serves as a template to examine the role of chlorine in a 3×3 chlorobenzamide isomer grid for direct comparisons with halogenated analogues.[31-42] In previous work, the effects of methyl or fluorine were analysed for comparisons in series of benzamides and pyridinecarboxamides using extensive physicochemical measurements.[43-46] Macrocycles derived from benzamides and devoid of strong hydrogen bond donors have been reported and the effect of halogen bonding on their 1D and 2D structures noted.[47-49] Herein, a series of nine chlorobenzamide (**Clxx**) isomers as $ClC_6H_4CONHC_5H_4N$ (**Scheme 1**) is presented. The nine compound **Clxx** series is synthesised from three *p*-/*m*-/*o*-chlorobenzoyl chlorides and three *p*-/*m*-/*o*-aminopyridine isomers using standard synthetic procedures: these are analogues of the fluorobenzamide (**Fxx**) isomer grid.[43] We present the structures,

conformational analyses and physicochemical properties of **Clxx**, together with highlighting correlations with crystal properties and molecular charge densities.

Materials, Methods and equipment

All chemicals, materials, vendors, spectroscopic and crystallographic methods together with computational programs and equipment are as noted previously.[43-46] Chemicals and silica (Davisil) were used as purchased from Sigma Aldrich, TLC alumina, silica plates from Fluka. Melting points were measured using a Stuart Scientific SMP40 automated melting point apparatus. IR spectroscopy was recorded using a Perkin Elmer Spectrum GX FTIR spectrometer by the ATR method: bands are quoted in cm^{-1}. NMR spectroscopy was performed on a Bruker BioSpin UltraShield NMR spectrometer (293±1 K), at 400 or 600 MHz for ^{1}H and 100.62 MHz for the ^{13}C resonance. The ^{1}H spectra were recorded in $CDCl_3$ with the ^{13}C spectra in $CDCl_3$. The NMR chemical shift values (δ) are in ppm, referenced to TMS and coupling constants (*J*) are quoted in Hz.

The single crystal X-ray data collections for all nine **Clxx** isomers as ten crystal structures (**Clpp**, **Clmp**, **Clop**, **Clpm**, **Clmm**, **Clom**, **Clpo_O**, **Clpo_N**, **Clmo**, **Cloo**; **Scheme 1**) together with data reduction, structure solution and refinements are typically routine.[43-46,50-52] Selected crystallographic and structural information are as detailed in the ESI (Tables S1, S2a-c, pgs 5-10)[51,53] with pertinent structural details provided in the main manuscript in **Tables 1**, **2**. Molecular and hydrogen bonding diagrams (**Figures 1-9**) are depicted with displacement ellipsoids drawn at the 30% probability level.[43,53,54] The computational calculations[55-57] are routine,[43-46] with optimisations and conformational analyses in *gas phase* as performed using the DFT method [B3LYP/6-311++G(d,p)].[56,57] All calculations were performed using Gaussian09[55] for Linux/Unix operating on a SGI Altix ICE 8200EX high performance computing system at the ICHEC (Galway, Ireland).

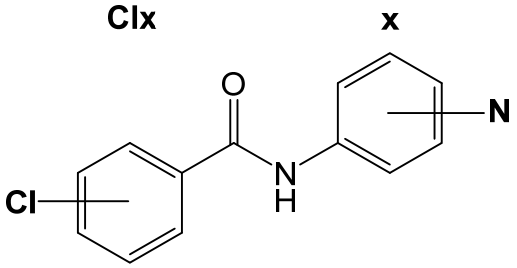

Scheme 1: The **Clxx** molecular structures with **Clx** representing the *p*-/*m*-/*o*-$ClC_6H_4C{=}O$ and **x** the *p*-/*m*-/*o*-HNC_5H_4N moieties (**x** = *para*-/*meta*-/*ortho*-substitution).

Table 1: Selected crystallographic data for **Clxx** (full details available; Table S1 in ESI)[50-54]

Structure	Crystal system; Space group	*Z'*	Unit cell volume (Å^3)	*R*, wR_2 factors
Clpp	Monoclinic; $P2_1/c$	1	1070.40(14)	0.038, 0.098
Clmp	Triclinic; $P\bar{1}$	4	2145.05(8)	0.039, 0.113
Clop	Orthorhombic; *Pbca*	1	2192.4(7)	0.041, 0.089
Clpm	Triclinic; $P\bar{1}$	4	2156.6(4)	0.043, 0.084
Clmm	Monoclinic; $P2_1/c$	1	1142.99(13)	0.050, 0.097
Clom	Monoclinic; *C*2/c	1	2256.16(9)	0.034, 0.089
Clpo_O	Monoclinic; *C*2/c	1	2134.8(3)	0.031, 0.089
Clpo_N	Monoclinic; *C*2/c	1	2222.78(5)	0.032, 0.093
Clmo	Triclinic; $P\bar{1}$	1	530.27(6)	0.034, 0.100
Cloo	Monoclinic; *C*2/c	1	2166.51(16)	0.036, 0.110

Footnote: *R*-factor definitions as $R[F^2 > 2\sigma(F^2)]$, $wR(F^2)$.[51]

Methods[58-62]

Electrostatic energy calculations were performed with the MoProSuite software.[58] The multipolar electron density of the molecules was modelled by transfer of the ELMAM2 charge density database without further refinement.[59] The asymmetric unit content was rendered electrically neutral after charge density transfer by applying a uniform valence population shift to all atoms. The N-H and C-H bonds were elongated to standard distances obtained from neutron diffraction.[60] The electrostatic energy is computed over pairs of atoms using the Hansen and Coppens multipolar atom model. The lattice electrostatic energy was computed with the VMoPro module in real space. The software can compute the energy in successive parallelepiped shells around the unit cell. Convergence was achieved over the [-9a,9a] × [-9b,9b] × [-9c,9c] space around the molecule containing 19^3 unit cells.

The Hirshfeld surface and decomposition of intermolecular contacts in pairs of chemical species were computed around the different moieties of the asymmetric unit with the program MoProViewer.[61] The polar H_N and hydrophobic H_C atoms were distinguished. Crystal contact enrichment ratios were averaged, as noted by Jelsch and Bisseyou:[62] arithmetically and harmonically, for values smaller and larger than unity, respectively.[62] Supplementary Figures and Tables are provided (ESI; Figures S4-S10; Tables S4-S7).

Table 2: Salient structural features (inter-planar angles, distances, packing; Å,°) of **Clxx**.[51]

Structure	**C_6/C_5N** (°)	**C_6/amide** (°)	**C_5N/amide** (°)	**N…N/O** (Å)	**Packing**
Clpp	50.88(6)	32.33(18)	19.2(2)	3.114(2)	1D chains
Clmp	10.98(9) 7.18(9) 5.19(4) 7.93(4)	33.47(6) 23.53(7) 1.11(5) 8.79(4)	22.80(7) 21.21(8) 4.54(5) 2.21(4)	2.9431(16) 3.0120(16) 3.1576(16) 3.1913(16)	1D chains
Clop	73.27(5)	64.64(6)	12.36(11)	3.010(3)	1D chains
Clpm	11.79(17) 11.54(16) 35.35(11) 33.24(10)	5.97(18) 6.25(17) 28.28(13) 27.57(13)	6.21(16) 5.33(16) 7.31(15) 5.78(14)	3.184(4) 3.203(4) 3.151(4) 3.150(4)	1D chains
Clmm	3.67(12)	21.71(8)	23.49(8)	2.892(4)* 2.858(4)* 2.890(4)*	N-H/O-H…O and O-H…O composites
Clom	74.97(4)	58.56(5)	17.13(5)	2.9058(17)	1D chains
Clpo_N	36.75(7)	35.80(7)	1.07(8)	3.0715(19)	Dimers
Clpo_O	3.44(8)	23.54(6)	20.92(6)	3.1296(14)	1D chains
Clmo	47.05(4)	36.25(4)	15.77(6)	3.1990(17)	Dimers
Cloo	66.72(4)	68.95(5)	2.90(3)	3.0485(14)	Dimers

Footnotes: C_6 is the (C11,...,C16) benzene ring and C_5N is the (C21,...,C26) pyridine ring defined for the least squares (LS) planes in **Scheme 2**; the bridging amide plane is defined as the 5 atom C_{ipso}-C(O)NC_{ipso} (or C11, C1, O1, N1, C21) LS plane, with reference to **Figures 1-9**. The **Clmp** and **Clpm** structures have *Z'*=4.
* = **Clmm** is a hydrate (hydrogen bonding distances all involve O1W).

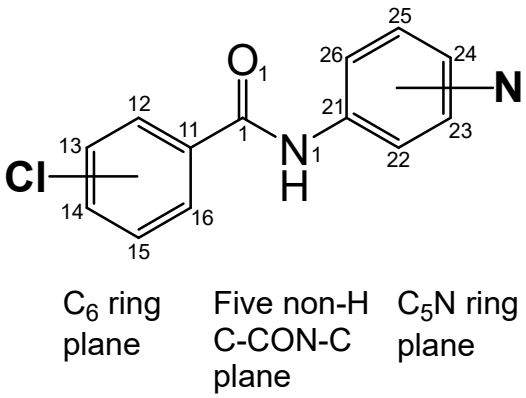

Scheme 2: A diagram of the three planes (with only non-hydrogen atoms used in the inter-planar calculations of **Tables 2** and **3**.

Results and Discussion

Crystal structure results:

Nine **Clxx** benzamide isomers are reported (as ten crystal structures), presenting a wide variety of molecular geometries and structures, with **Clpo** or *para*-Chloro-*N*'-(*ortho*-pyridyl)benzamide crystallizing as the **Clpo_N** and **Clpo_O** polymorphs ($\mathbf{N}_{pyridine}$ or $\mathbf{O}_{amide}$ suffixes denote the primary intermolecular hydrogen bonding acceptor). There is isomorphous overlap between some **Clxx** structures with their **Fxx**,[43] **NxxF**,[44] **Mxx**[45] or **NxxM**[46] isomer grid relatives (ESI, Figures S1,S2) and there is also structural similarity with the **CxxM** and **CxxOMe** carbamates.[63,64] Computational studies in *gas phase* are analysed for comparisons directly with the crystal structure results.[43-46,55-57] Only salient features of each **Clxx** structure are presented, with further information in the ESI (Tables S1, S2a-c).

The Clpp, Clmp, Clop series: Isomorphism

Clpp (**Figure 1**) crystallises in the monoclinic system (space group $P2_1/c$, with Z=4) and augments a series of seven isomorphous compounds that includes the parent **Hpp**,[65] the **Fpp**, **Fmp**, **Fop** triad (Figure S2, ESI),[43,66] **25p**,[67] **Clpp** and **Brpp**.[68] These molecules display varied peripheral H/F/Cl/Br atom-site positions and the resultant isomorphous series is unusual in that the structures have similar unit-cell parameters, packing and alignment but different interaction/contact geometries at the secondary level.[43-46,69-72] Disparities are primarily due to the 0.3–0.7 Å differences between typical organic C-H/F/Cl/Br bond lengths (Å) and resulting directional influence of the peripheral **X** atoms on weaker interactions and contacts in their respective crystal structures. With increasing numbers of structures available on the CSD,[40-42] it is expected that progress will be made towards forming a *continuum* where isomorphous series of molecules overlap with series of isostructural compounds. In fact, **Mpp** (*para*-Methyl-*N*'-(*para*-pyridyl)benzamide) bears a resemblance to **Clpp** and is considered as an isostructural relative.[45] In the literature there is considerable on-going interest on groups of isomorphous structures that exhibit structural diversity.[69-72]

The **Clpp** structure contains an intramolecular C26-H26…O1 contact (C26…O1 = 2.891(2) Å, C-H…O = 117°). The classic N-H…N intermolecular interaction [N1…N24^{i} = 3.114(2) Å, 139.2(17)°; symmetry code i = 1-x, y+½, ½-z, ESI, Table S2a] with $C(6)$ motif is the principal hydrogen bond and the remaining intermolecular interactions comprise C-H…O [3.3482(2) Å, 130°] and Cl14…C(π) halogen bonding contacts [3.3269(18) Å, C14-Cl14…C21^{xix} = 150.10(7)°; symmetry code *xix* = x,½-y,½+z],[31-39] linking the non-planar molecules into a 3D structure (**Figure 1**), together with C-H…π and aromatic stacking.[25,27,30] **Clpp** forms part of an isomorphous series that widens the structural scope of a group of similar structures.[40]

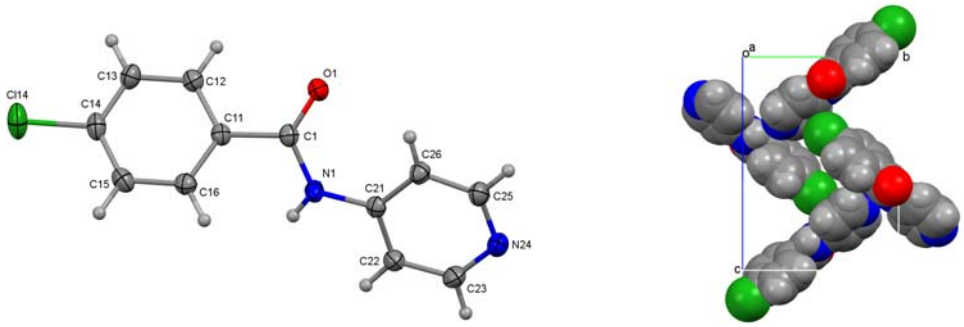

Figure 1: ORTEP of **Clpp** and CPK view of the N1-H1…N24 and C14-Cl14…C(π) contacts.[31-39]

Clmp crystallises in the triclinic system (space group $P\bar{1}$, with Z=8), containing four independent molecules in the asymmetric unit (Z'=4)[73-75] (**Figure 2**). Trials in a subunit cell (with *c*-axis halved) in $P2_1/n$ gives a result with R = 0.11 having at least four non-H atoms with unusual displacement ellipsoids; this result was discarded. In **Clmp** the major differences between all four molecules (**A**, **B**, **C**, **D**) are exemplified by different O=CCC torsion angles [with a range >30°, from 144.06(14)° to 177.91(13)°] and distinct N1-H1…N24 distances [~0.25 Å, from 2.9431(16) Å to 3.1913(16) Å]. However, the (**A**, **B**) and (**C**, **D**) molecules form distinct pairs that are broadly similar in conformation (**Table 2**). The aromatic rings in **Clmp** twist by between 5° and 11° relative to each other (*i.e.* by 5.19(4)° in **C**; 10.98(9)° in **A**), whereas the amide group is twisted away from both aromatic rings in molecules **A** and **B** only, as molecules **C** and **D** are essentially planar. The chlorine atom is located as **Cl-*syn*** relative to the amide N-H (as for **Fmp**).[43] An intramolecular contact is present as C22-H22…O1 in all four molecules in a *d*(C,O) range from 2.8073(17) to 2.8709(16) Å, with angles 115° to 121°. Molecules aggregate by N-H…N intermolecular interactions as **A**→**D**→**A**→**D**… and **B**→**C**→**B**→**C**… alternating pairs. The N1…N24 distances are 2.9431(16), 3.1913(16)^{iii} Å (for **A**, **D**) and 3.0120(16), 3.1576(16)^{ii} Å (for **B**, **C**) with the *C*(6) motif forming *zigzag* chains parallel with (001). In addition parallel offset amide…arene stacking contributes to structural stability and packing, especially involving centrosymmetric related **C** molecules with short **C**…**C** contact distances of 3.32, 3.36 Å.[30] Weaker intermolecular C-H…N/O hydrogen bonds also influence with C-H…N playing an auxiliary role to the N-H…N, in addition to weak C-H…Cl contacts.[25-30] Molecules stack with the relatively planar (**C green**, **D yellow**) molecular pairs along the *c*-axis direction as (**C**…**C**…**D**…**D**…) and forming a herringbone arrangement with the **A** (**red**) and **B** (**blue**) pairs (packing diagram). The **Clmp** crystal structure contains two slightly different molecular geometries and stacking sequences in the (**A**, **B**) and (**C**, **D**) pairs with packing influences from the N-H...N hydrogen bonded chains and parallel offset π…π stacking effects.[30] This may be a contributing factor in the isolation of the **Clmp** crystal structure with Z'=4.[73-75]

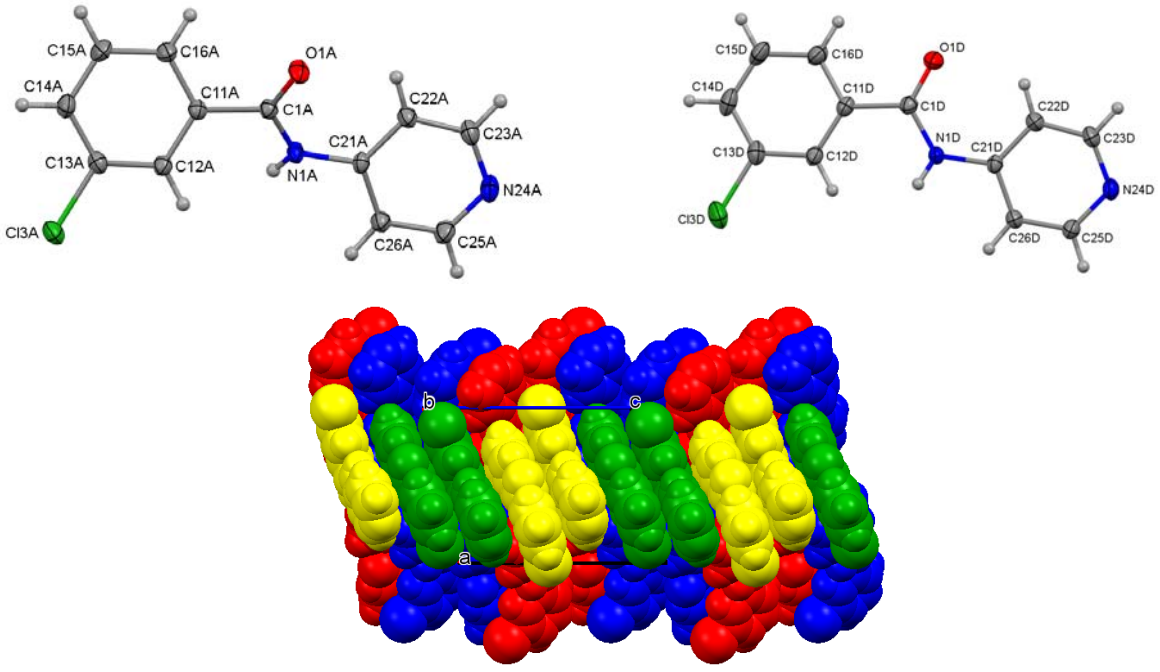

Figure 2: ORTEPs of **Clmp** (molecules A and D, top) and a CPK packing view (**A**, **B**, **C**, **D**).

Clop is isomorphous with the **Brop** crystal structure.[68] Molecules of **Clop** twist from non-planar geometry (**Figure 3**) due to the influence of the *ortho*-Cl12 atom (~**Cl-*syn***) but the amido-pyridine group remains essentially planar due to the C26-H26…O1 intramolecular contact. **Clop** aggregates by intermolecular N1-H1…N24 hydrogen bonds into 1D chains [as *C*(6)] that are further linked into 2D sheets parallel with (001) by Cl12…O1^{xxi} halogen bonding interactions [Cl12…O1^{xxi} = 3.1104(18) Å; N_c = 0.95],[31-39] with C12-Cl12…O1 = 161.09(8)°, Cl12…O1=C1 = 111.27(12)°. The N-H…N interaction geometry is regular with N1…N24^{vi} = 3.010(3) Å (N1-H1…N24^{vi} = 175.9(18)°), but the orientation is skewed towards 120° with N1…N24^{vi}…C21^{vi} (= 137°). A C15-H15…O1^{vii} interaction is also noted.

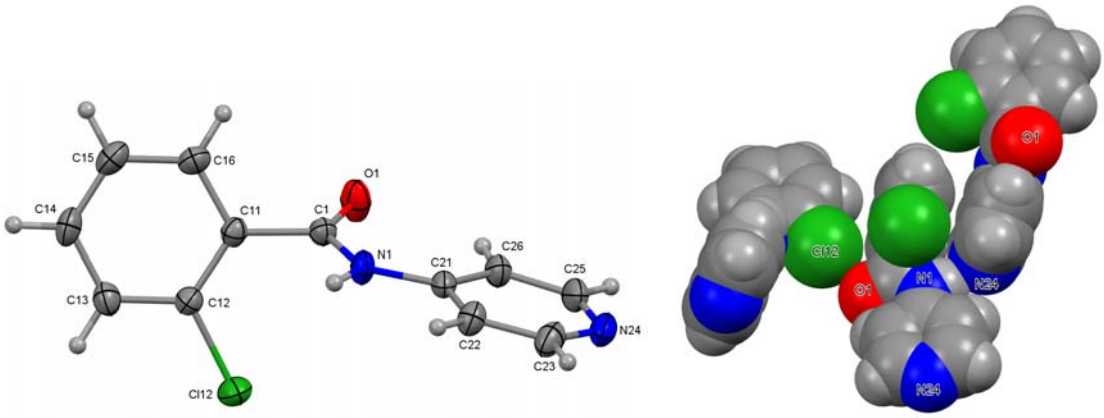

Figure 3: ORTEP of **Clop**; CPK view of the N1-H1…N24^{vi} interaction, Cl12…O1=C1^{xxi} contact.

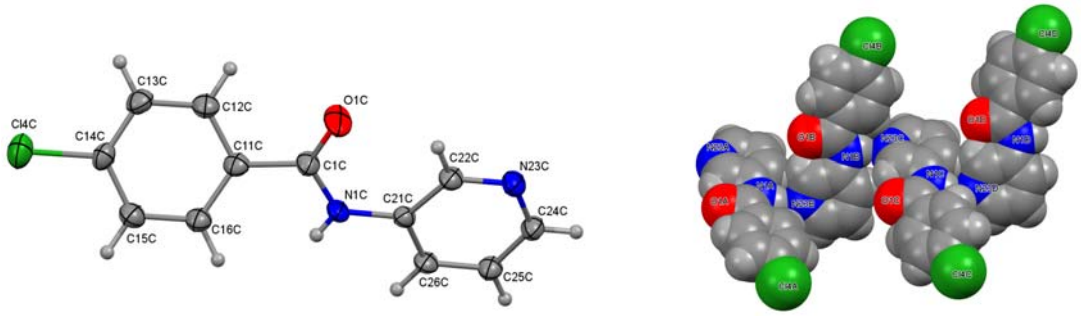

Figure 4: ORTEP of **Clpm** (molecule C) and a CPK view of the N1-H1…N23 chain.

The Clpm, Clmm, Clom series: twinning and isomorphous behaviour.

Clpm is a twinned structure with four molecules (A to D; *Z*'=4)[73,75] (**Figure 4**), assigned as (A, B) and (C, D) pairs in the asymmetric unit and differing slightly in their inter-planar C_6/C_5N angles of 11.93(15)°, 11.78(14)°, 35.29(10)° and 33.18(9)°. Geometrical differences are noted by intermolecular $C16_{A/B/C/D}$…$C24_{B/C/D/A}$ contacts of 3.743(5) Å, 3.709(5) Å, 3.774(5) Å, 3.834(5) Å along the $(A\rightarrow B\rightarrow C\rightarrow D\rightarrow)_n$ hydrogen bonded chains as linked by modest N1-H1…N23 interactions (**Table 2**). The N…N range is 3.150(4) to 3.203(4) Å and assisted by flanking $C16_{A/B/C/D}/C26_{A/B/C/D}$…$N23_{B/C/D/A}$ interactions and contacts (with **P-*anti***). Additionally C-H…Cl/O/π weak hydrogen bonds augment the intermolecular contacts.[25-30,40] Crystal structures with *Z'*=4 are uncommon though not unusual and have been encountered in related series;[40-42,73-75] **Mpm** crystallises in the triclinic system (space group *P1*, with *Z*=*Z*'=4),[45] **NmpF**[44] and **Clmp** likewise (space group $P\bar{1}$, with *Z*=8 and *Z*'=4). One can surmise

that two independent molecules (*Z'*=2) can be accommodated by N-H…N interactions in a 1-D chain. Statistically, structures with *Z'*=4 are considerably less likely to arise.[40-42,73-75] The cumulative effects and strengths of aromatic stacking[30] together with intermolecular contacts *e.g.* $C16_{A/B/C/D}$…$N23_{B/C/D/A}$ may have a subtle but important impact on intermolecular organisation and packing.[25-30]

The **Clmm•**(H_2O) monohydrate is isomorphous with **Brmm•**(H_2O).[68] The **Clmm•**(H_2O) structure crystallises with three main hydrogen bonds driving aggregation using N1-H1…O1W^{ix}, O1W-H2W…O=C^{i} and O1W-H1W…N23.[25-30] The former two interactions combine to form a $R^4_4(12)$ assembly with two H_2O molecules sandwiched between two **Clmm** (as **Cl-*syn***; **P-*syn***) (**Figure 5**). The remaining O1W-H1W…N23 interaction links tetrameric [**Clmm•**(H_2O)]$_2$ assemblies *via* the pyridine N23 atom; each tetramer has two O1W-H1W donors and N23 acceptors for a total of four hydrogen bonds per assembly. Hydrogen bonding is maximised whereby three donor groups (N-H, 2 × O-H) and three acceptors (O=C, O, N) participate with water playing a critical role in aggregation. In our isomer grids, benzamide hydrates are usually obtained from recrystallization in halogenated solvents or ethyl acetate.[43-46] They tend to have a *meta*-$N_{pyridine}$ atom favouring hydrogen bonded ring formation with water molecules incorporated (adventitiously) between benzamides.

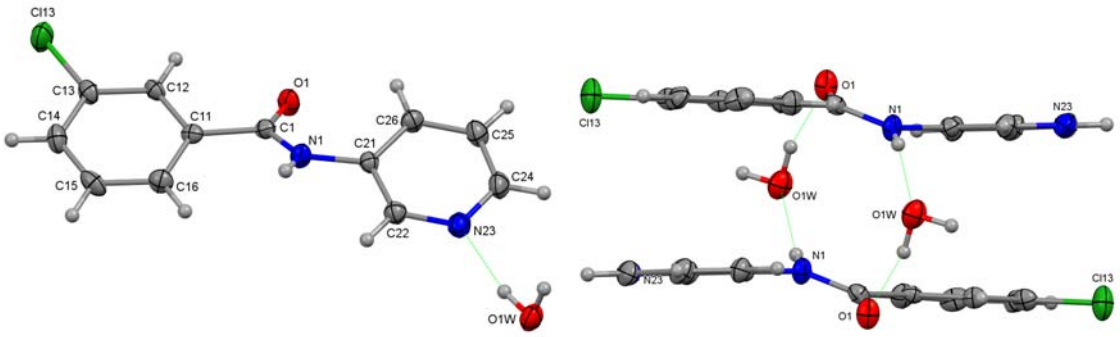

Figure 5: ORTEP view of **Clmm•**(H_2O) and $R^4_4(12)$ assembly of **Clmm** with H_2O molecules.

Clom adopts a (**Cl-*anti***; **P-*anti***) conformation with an intramolecular C22-H22…O1 interaction [2.8845(19) Å, 120°)] and Cl12…O1 contact [Cl12…O1 = 3.1811(13) Å] (**Figure 6**).[25-39] **Clom** is isomorphous with **Brom**,[68] and is similar in structure to **Mom** (**M-*anti***; **P-*anti***) aggregating with N-H…N chain formation.[45] This arrangement contrasts with **Fom** (**F-*syn***; **P-*anti***)[43] having two intramolecular C-H…O contacts, an intramolecular N-H…F interaction and weak N-H…O=C chain association. As such, **Clom** molecules do not exhibit intramolecular N-H…Cl interactions but assemble by N-H…N interactions as 1-D chains along the *c*-axis direction. These are weakly linked into 2D sheets by C-H…O interactions and with type I halogen…halogen C_{arom}-Cl…(Cl-C_{arom})^{xxiv} interactions of 3.3699(10) Å (**Figure 6**); though considerably longer than the aromatic C-Cl…Cl-C contact of 3.165(3) Å noted in (**ClIO**)$_3$.[49] The trade-off in interactions works for **Clom** and one can postulate that differences between **Mom**,[45] **Fom**,[43] and **Clom** derive from an intricate balance between intramolecular (mainly N-H…F interactions for F in **Fom**) and intermolecular (mainly N-H…N formation for Me

(**Mom**) and Cl (**Clom**)) forces. It also suggests that that in terms of aggregation, the **Fom** polymorphs are rather unexpected and influenced by intramolecular forces.[43]

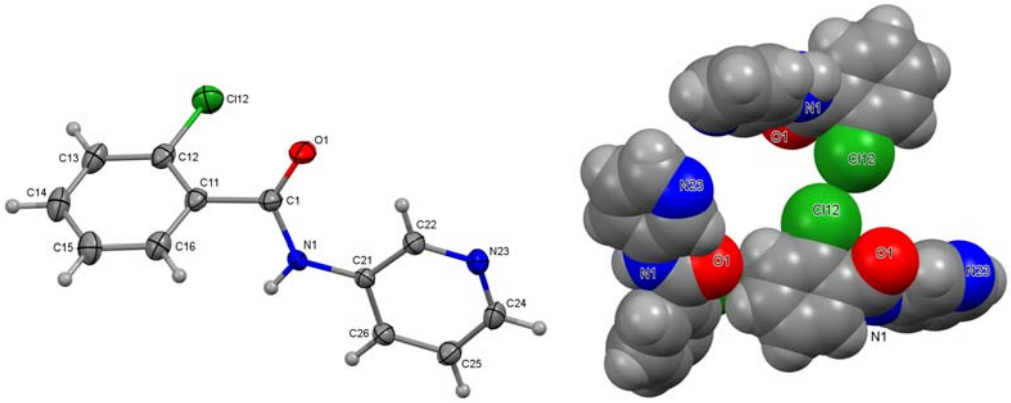

Figure 6: ORTEP of **Clom** and a CPK view of the Cl12…Cl12[xxiv] and C-H…O contacts.

The Clpo, Clmo, Cloo series: polymorphism in Clpo (**Clpo_O** *and* **Clpo_N**)[76-80]
Clpo crystallises as two polymorphs, both **P-*syn***, (**Figures 7, 8**; monoclinic system, space group *C2/c*, with *Z*=8: *Z'*=1). Thus **Clpo_O** (from ethyl acetate) forms intermolecular interactions as (*i*) N-H…O=C interactions in *C*(4) chains along the *b*-axis direction with N1…O1[xi] = 3.1296(14) Å, (*ii*) parallel offset ring stacking interactions with C1…C16[xxv] = 3.3488(19) Å and (*iii*) C15-H15…N22[xii] interactions forming dimers [3.5199(19) Å] as $R^2_2(16)$ rings.[25-30] **Clpo_O** with amide…amide interactions is distinctly different to the related *ortho*-pyridine (**Yxo)** structures (**Y** = **Me**,[45] **F**,[43] **Cl** (see below), **Br**), *e.g*. **Mxo**, **Fxo** (**x** = *para*-, *meta*-, *ortho*-) which aggregate as cyclic N-H…N hydrogen bonded dimers.[43,45] The pyridine *ortho*-N atom facilitates the formation of compact $R^2_2(8)$ rings in the six **Mxo** and **Fxo** structures (as **P-*syn***) with secondary interactions, *e.g*. interdimer interactions completing the structural interactions. The driving force towards **Yxo** hydrogen bonded dimer formation remains, and with a range of geometries available, despite both intramolecular (C-H…O) and intermolecular interactions competing (as above) to potentially disrupt dimer formation. **Clpo_O** though forms weakly held dimers that are comparable with the related **Fpm_O** [$R^2_2(18)$],[43] nevertheless with a smaller hydrogen bonded ring size (16 atoms *vs* 18 atoms).

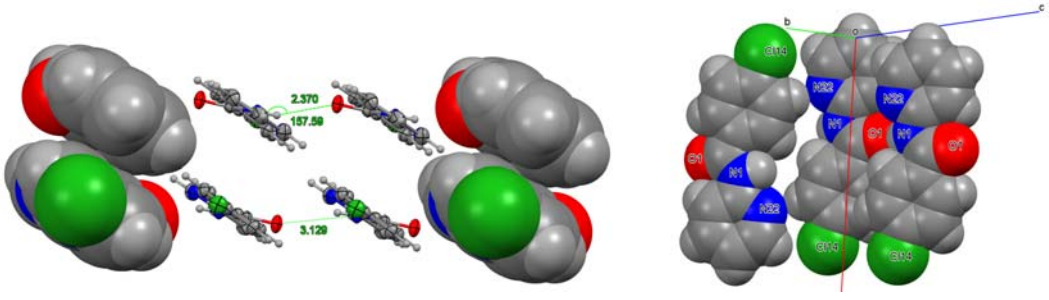

Figure 7: Views of **Clpo_O** with N-H…O=C and aromatic stacking interactions (*left*) and intramolecular C-H…O interactions and intermolecular C-H…N contacts (*right*).

Unexpectedly, and from crystallisation experiments attempts to obtain a series of benzamide hydrates, the **Clpo_N** polymorph was isolated from a mixture of acetonitrile and water. **Clpo_N** aggregates as hydrogen bonded N-H…N dimers (and similar to the six **Fxo**,

Mxo),[43,45] linked together into a 1-D chain by weak C-H…O contacts, further linked by C-H…O contacts aligning along the *c*-axis direction. The anticipated **Clpo_N** structure has a lower than expected KPI (packing index) of 67.1 compared to 70.0 for (**Clpo_O**) and this is due to the presence of voids in **Clpo_N** (**Table 3**).[53] Analysis of the **Clpo_N** molecular packing shows channel formation but these voids are barely large enough to accommodate a hydrogen atom or H_2 molecule (**Figure 8**). In summary, there is a trade-off in crystallising **Clpo** as (*a*) **Clpo_O** with an increased number of moderate strength interactions (N-H…O=C, C-H…π, N and C…C stacking) and optimum packing (70.0) at the expense of (*b*) the stronger expected N-H…N cyclic dimer formation in **Clpo_N** with looser packing (67.1). Of note is compound **ROY** which is an extraordinary example of a molecular compound having ten polymorphs isolated to date.[78] In **ROY** there are four polymorphs crystallising in the monoclinic system (space group $P2_1/c$) making it rather unusual to have a high number of polymorphs as a subset in one space group.[78]

Table 3: Differences between the **Clpo_O** and **Clpo_N** polymorphs (in Å,°).[a]

Polymorph	KPI[53]	C_6/C_5N (°)	N-H…N/O (Å,°)	C-H…N/O (Å,°)[b]	C-H…O (Å,°)[b,c]
Clpo_O	70.0	3.44(8)	3.1296(14)[xi], 157.7(15)	3.5199(18), 168	2.8954(17), 116
Clpo_N	67.1	36.75(7)	3.0715(19)[xiii], 162.4(17)	3.329(2), 129	2.840(2), 121

[a] = Packing index KPI from PLATON[53]; aromatic interplanar angles C_6 is the C_6 benzene ring, C_5N is the 6 non-H atom of the pyridine ring in **Scheme 2** (°); primary hydrogen bonding distances in (Å), angles in (°).
[b] = Aromatic C-H hydrogen atoms as riding atoms in refinement and without esd's.
[c] = Intramolecular C26-H26…O1 contact (distances in Å; angles in °).

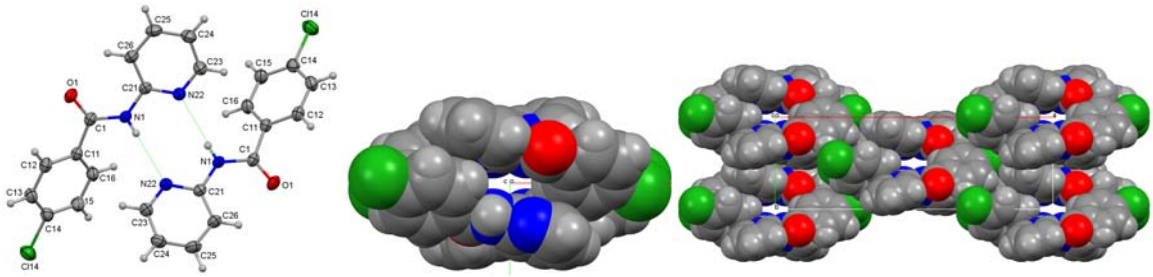

Figure 8: The cyclic dimer in **Clpo_N** with CPK views of the voids along the *c*-axis.

Clmo aggregates as cyclic N-H…N hydrogen bonded dimers and N-H…π contacts (with slipped/stepped aromatic rings; **Figure 9**), contrasting with **Clpo**, though similar in molecular structure (dihedral angles) to **Mpo**.[45] The N1…N22[xv] distance of 3.1990(17) Å is the longest in the nine **Yxo** hydrogen bonded dimers reported to date (for **Y** = **Me**, **F**, **Cl**).[43,45] The **Mxo** triad[45] forms symmetrical, planar dimers about inversion centres, whereas the **Fxo** series[43] aggregate as twisted hydrogen bonded dimers in **Fpo** (about a 2-fold axis) and with two independent molecules in the asymmetric units of **Fmo**, **Foo** (both crystallising in the triclinic system, space group $P\bar{1}$). Of further note in **Clmo** is the lack of halogen bonding interactions of any consequence involving the chlorine atom Cl13, which is exclusively surrounded by several C-H atoms (ESI: Tables S4-S5).

Cloo is isomorphous with **Broo**,[68] and forms N-H…N hydrogen bonded dimers about 2-fold axes and is similar in conformation to **Foo**.[43] Compact parallel offset heterocycle stacking

interactions involving the *ortho*-pyridine rings dominate with short C24…C26[xxvii] distances of 3.3049(18) Å about inversion centres (**Figure 9**). In tandem, C-H…π(arene) contacts arise involving the aromatic C16-H16 and C23-H23 moieties with symmetry related benzene rings. The aggregation can also be viewed as **Cloo** dimers that stack in columns in the *b*-axis direction with tight pyridine...pyridine stacking interactions contributing to form tightly interwoven 2-D sheets. For comparisons, although both **Clmo** and **Cloo** exhibit regular behaviour in their respective aggregation, for all three **Clxo** isomers the carbonyl atom O1 has barely any influence on molecular aggregation.

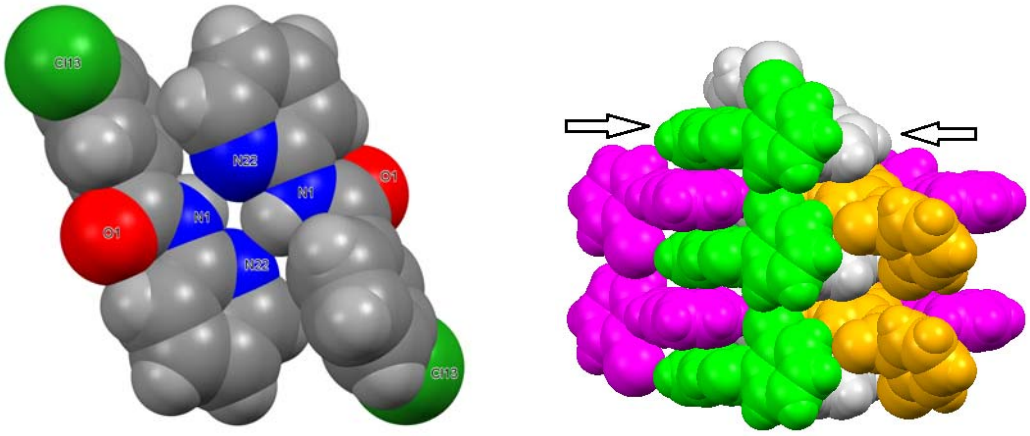

Figure 9: The **Clmo** dimer and pyridine…pyridine ring parallel stacking interactions in **Cloo**.

Summary of the Clxx solid-state structural results

The notable structural results for the **Clxx** series are: (*i*) the **Clpo_O**, **Clpo_N** polymorphic pair[76-80] (both as *Z*'=1 in space group *C2/c*) and with voids present in the **Clpo_N** polymorph, (*ii*) the **Clmp** and **Clpm** structures having a relatively high *Z*'=4 in the asymmetric unit,[73-75] which is rather uncommon in benzamide structures reported to date,[43] and (*iii*) the distinct lack of intermolecular Cl…O and Cl…N halogen bonding, apart from clear-cut cases such as **Clop** (as aromatic C-Cl…O=C interactions) and **Clom** (with aromatic C-Cl…Cl-C contacts). There is, however, a C-Cl…π intermolecular contact where the Cl σ-hole faces the pyridine ring in **Clpp** at an angle (C-Cl, π ring centroid) = 163.34(7)°.[31-39]

The **Clxx** isomer grid places in context the structural relationships that exist between isomer grids, *e.g*. **Mxx**,[45] **Fxx**[43] and **Brxx**.[68] Overall, the structural landscape is broad, but overlaps include (*a*) five **Clxx** isomers that are isomorphous with their **Brxx**[68] analogues as the **Clpp**/**Brpp**, **Clop**/**Brop**, **Clmm**/**Brmm** monohydrates, **Clom**/**Brom** and **Cloo**/**Broo** pairs, and (*b*) the **Clpp** isomer being isomorphous with several related structures, including the parent **Hpp**,[65] **Fpp**, **Fmp**, **Fop** triad,[43,66] **25p**,[67] **Clpp** and **Brpp**.[68]

Our results show the considerable overlap between the **Clxx** and **Brxx**[68] structures and greater differences with their **Fxx** and **Mxx** isomer grid analogues.[43,45] The only molecular series where there is continuity between the structures is for the **Xpp** series, which is extensive at the isomorphous and isostructural level, especially so as it overlaps with **Fpp**/**Fmp**/**Fop** triad. Subtle differences at the molecular level do not impact on the overall

molecular aggregation (isomorphous series) and differences between the crystal structures are noted at the secondary level.[40-42,65-72]

Why is there such a considerable overlap between Clxx, Brxx but not with Fxx or Mxx?

In order to quantify the isomorphous relationships in the isomer grids studied to date, **Table 4** is presented and highlights the isomorphous behaviour and relationships between various **Yxx** benzamide structures (**Y** = **Me**,[45] **F**,[43] **Cl**,[this work] **Br**[68]; **x** = *para-*, *meta-*, *ortho-*).[40-42,66-72] Another set of relationships is to be expanded upon in the **Clxx**/**NxxCl** isomer series in future papers in addition to the **Brxx** and **NxxBr** series (**NxxCl** and **NxxBr** are the amide bridged reversed isomers of **Clxx** and **Brxx**, respectively).[68]

Table 4: Isomorphous relationships in several series of benzamides[40-46,68]

Other	**Fxx**[43]	**Clxx**	**Brxx**[68]	**Mxx**[45]
Hpp[65]	**Fpp**	**Clpp**	**Brpp**	***Mpp***
25p[67]	**Fmp**	Clmp	Brmp	Mmp
	Fop	**Clop**	**Brop**	Mop
	Fpm	Clpm	Brpm	Mpm
	Fmm	**Clmm***	**Brmm***	Mmm
	Fom	**Clom**	**Brom**	Mom
	Fpo	Clpo	Brpo	Mpo
	Fmo	Clmo	Brmo	Mmo
	Foo	**Cloo**	**Broo**	Moo

Isomorphous pairs highlighted in **colour**. * crystallises as a monohydrate

Table 4 highlights the significant overlap in isomorphous behaviour between 5 of the 9 pairs of structures (55%) in the **Clxx** and **Brxx** isomer grids.[68] This is not altogether unexpected and the isomer series as presented demonstrates mutual similarities and differences with their **Fxx** and **Mxx** analogues. Another group is the *para-para* series (**Ypp**) spanning at least seven benzamides from the parent **Hpp** to **Brxx**, with differences only obvious at the secondary interaction level.[40-42,65,68-72]

A question arises as to why is there so much structural overlap between the **Clxx** and **Brxx** analogues? This can be addressed by comparing our results with a CSD[40-42] study by Mukherjee and Desiraju in 2014,[34] in which they analysed a series of Cl/Br-containing structures where the pairs differ by replacement of a C-**X** (**X** = Cl or Br).[34] In providing an insight into the behaviour of analogous pairs their statistical analysis highlights a high degree of similarity between both sets and with ~57% of the C-Cl/Br pairs sharing the same space group, *Z* and reduced cell parameters (within 1 Å). In their comprehensive study,[34] the relative absence of Cl…Cl (or Br…Br) contacts was further noted and only observed in <8% of structures (including disorder, classification ambiguities and Cl…Br interactions). Our

present results and statistics (~55%) therefore correlate well with those reported from Mukherjee and Desiraju.[34,40-42] The interchange of Cl/Br in the majority of structural pairs from the Mukherjee and Desiraju CSD study,[40-42] does not result in major structural changes or diversity and hence the high degree of structural overlap.[34,40-42]

Ab initio modelling and conformational analyses

In order to investigate the modelled, optimised structures of the nine **Clxx** molecules and differences with their solid-state molecular structures, optimisation of the modelled **Clxx** molecules was performed using the *ab initio* software Gaussian09[55] based on the DFT method (hybrid density functional B3LYP with 6-311G++(d,p) basis set, *gas phase*).[56,57] Models with optimised geometries (**Table 5**) were then used in the conformational analysis procedure.[43-46] Each of the **Clxx** structures was subject to full Potential Energy Surface (PES) scans (±180°, increment of 5°) of the two key C12-C11-C1=O1 (α, **Cl**-ring) and C1-N1-C21-C26 (β, **P**-ring) dihedral angles. Each of the asymmetric (*meta*- or *ortho*-) chlorophenyl (**Cl**-ring) or pyridine (**P**-ring) groups, can adopt, relative to the amide linker, two conformations (***syn*** or ***anti***) (**Scheme 3**), as denoted by ***syn*** (**Cl-*syn***, **P-*syn***) or ***anti*** (**Cl-*anti***, **P-*anti***). Aromatic rings with a *para*-pyridine N and/or *para*-phenyl Cl atoms are not subject to this convention. The results provide nine diagrams with two PES curves highlighting the conformational preferences (***syn*/*anti***) and with the rotational barriers for both dihedral angles in kJ.mol^{-1}.[43-46,63-64]

Table 5: Torsion angles (°) of optimised **Clxx** isomers[a]

Clxx	α/°	β/°	δ/°
Clpp	-24.41	-5.29	-2.90
Clmp	26.57	5.26	2.89
Clop	32.98	-1.52	3.19
Clpm	-24.17	-5.65	-2.31
Clmm	26.50	6.05	2.19
Clom	-32.75	0.94	-3.10
Clpo	-21.57	-3.63	-2.34
Clmo	22.16	2.96	2.56
Cloo	37.22	0.07	3.06

[a] Angle C12-C11-C1=O1 (**Cl**-ring) is α; angle C1-N1-C21-C26 angle (**P**-ring) is β and the O1-C1-N1-C21 angle (amide linkage) is δ. All geometries are based on B3LYP/6-311++G(d,p) optimisation in *gas phase*.[56,57]

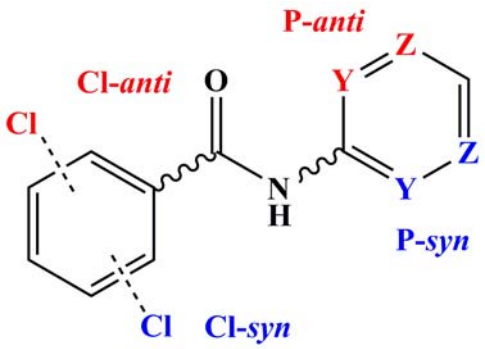

Scheme 3: The four possible **Clxx** conformations for the ClC_6H_4 and C_5NH_4 pyridyl rings.

The conformational diagrams of the **Clxx** *gas phase* modeled structures (**Figure 10**) have PES curves for the **P**-rings (pyridyl, β dihedral angle) depicted as **full red** lines and **Cl**-rings (chlorophenyl, α dihedral angle) as **blue dashed** lines. The *x*-axis shows the dihedral angle difference (θ) against the optimized dihedral angle in degrees (θ = 0° is the dihedral angle in

its optimized state, **Table 5**) and *y*-axes are the relative energies (ΔE) in kJ.mol^{-1}. At θ = 0° and ±180°, the asymmetric **Cl**- or **P**-ring conformation is denoted as either ***syn*** or ***anti***.

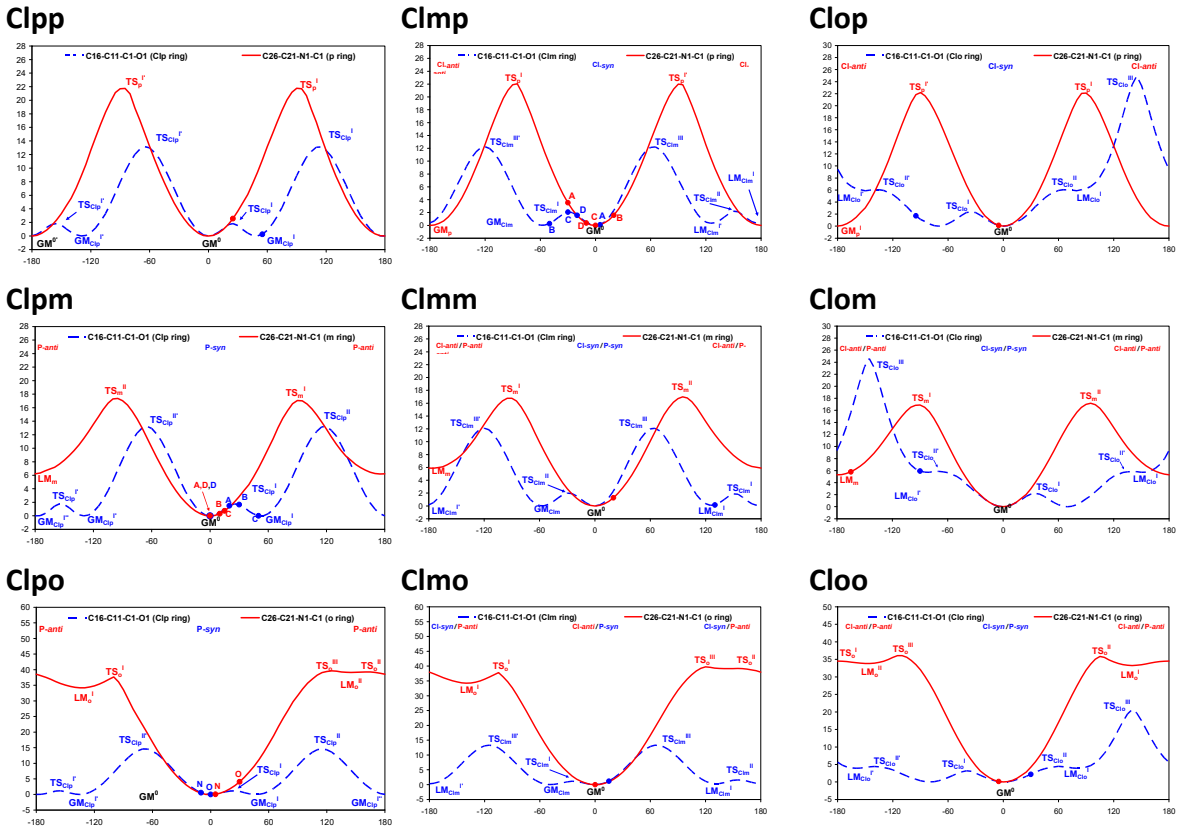

Figure 10: The Potential Energy Surface conformational analysis for nine **Clxx** optimized in the *gas phase*: the equivalent solid-state angle is shown by (•) with, if applicable, an assigned identifier. Enlarged versions are available in the ESI (Figure S3).

The geometry optimization and conformational analysis of the nine **Clxx** structures reveals several interesting observations. Firstly, the optimized **Clxx** geometries more closely resembles the methylbenzamide (**Mxx**)[45] isomer grid than the related fluorine analogues (**Fxx**).[43] The **Clox** triad is not planar like the equivalent **Fox** triad.[43] This is mainly due to the absence of intramolecular N-H…Cl hydrogen bonding in the former and to the presence of intramolecular N-H…F interactions in the latter. However, the **P**-ring is still co-planar with the amide linker plane. In addition, the **Cl**-ring in the **Clox** triad exhibits a greater deviation from planarity, as already noted in the **Mox** triad,[45] since the Cl atoms in the **Clox** triad do not form intramolecular hydrogen bonds with the amide N-H as the latter moiety prefers to interact with strong hydrogen bond acceptors such as amide C=O and pyridine N atom. It is interesting also to note that the **Clmo** calculations suggest that the **Cl-*anti*** conformation is more stable than the **Cl-*syn*** conformation as would be expected.

The height of rotational barriers (energy differences) is comparable with the equivalent PES diagrams in the **Fxx** isomer series as well as for **P**-rings in **Mxx**.[45] The profiles of the **Clo**-rings are asymmetric, though similar in shape to the **Fo**-rings (which are symmetric due to planarity/hydrogen bonding) and with slightly lower energy barriers. The **Clp** and **Clm** PES diagrams are very similar both in shape and barrier height to the **Fp** and **Fm** rings in **Fxx**.[45]

In each PES curve in **Figure 10** the position of the solid-state dihedral angles of the **Cl-** and **P-**rings are marked by a dot (either • or •) and if there is more than one molecule/polymorph these are marked with a corresponding letter. These marks illustrate the deviation of the solid-state angles from the optimized ones (at $\theta = 0°$) and from the closest global minimum. In most of the nine **Clxx** isomers there are small deviations (+/-30°) from the optimized starting points or closest minima, and up to *ca*. 3-4 kJ.mol^{-1} of energy difference. Although for **Clmm** and **Clop**, energy differences from the most stable conformer are noticeable, in general, there are no significant deviations between the global minima except for **Clom**.

In **Clmm** the most stable conformer *in vacuo* is **Cl-*syn*** but the **Cl-*anti*** conformation is observed in the solid-state. This conformational change from **Cl-*syn*** to **Cl-*anti*** is necessary to allow the formation of N1-H1…O1W hydrogen bonding that is essential for molecular aggregation in the crystal structure. If the **Clmm** molecule retained the **Cl-*syn*** conformation, then formation of this hydrogen bonding arrangement would be hampered. In the **Clop** crystal structure the **Clo**-ring deviates by ~90° from its gas phase optimized minimum and is positioned between the **Cl-*syn*** and **Cl-*anti*** conformation. However, the energy expense of this deviation is just ~3 kJ.mol^{-1} and the angle change (deviation) is preferred as it facilitates the C12-Cl12…(O1=C1)^{xxi} halogen bonding and C15-H15…O1^{vii} hydrogen bonding formation.

In the **Clom** crystal structure the *meta*-pyridine ring adopts the unfavorable **P-*anti*** conformation which is ~5 kJ.mol^{-1} higher in energy than the alternative **P-*syn*** conformation. This conformational change is also seen in **Brom**[68] and **Mom**[45] and allows the formation of regular hydrogen bonded N-H…N *zig-zag* chains. There is a chlorine…chlorine contact which is almost in a head-to-head geometry as C12-Cl12…Cl12 = 167.66(6)°; see ESI (Figure S10). This configuration seems unfavourable at first glance as the two σ-holes are almost oriented towards each other. Moreover, the electrostatic energy from the deformation electron density part is indeed positive ($E_{\text{elec-Def}}$(Cl…Cl) = +0.8kJ.mol^{-1}). However, as the neutral spherical atom contribution ($E_{\text{elec-Neu}}$ = -4.5kJ.mol^{-1}) is very negative and the penetration energy (cross term describing the interaction between deformation and neutral spherical components) is very small, the interaction is globally stabilized from an electrostatic viewpoint (E_{elec} = -3.5kJ.mol^{-1}).

In general terms, conformational analysis of the nine **Clxx** isomers exhibits agreement between the conformations of the solid-state and modeled molecular structures, apart from the **Clop**, **Clmm** and **Clom** isomers (as noted above in the PES diagrams, **Figure 10**). These findings are consistent with our previous results in similar, related isomer grids though the optimized **Clxx** geometries more closely resemble the methylbenzamide (**Mxx**)[45] isomers than the related fluorine analogues (**Fxx**).[43]

Melting point analysis:[81-89] comparisons with related series

For the **Clxx** series, it is noted that Carnelley's rule[81] is adhered to on symmetry grounds with the most symmetrical **Clpp** (*para*-Chloro-*N*'-(*para*-pyridyl)benzamide) having the highest melting point (mp = 207°C) and the unsymmetrical **Clmo** (*meta*-Chloro-*N*'-(*ortho*-pyridyl)benzamide having the lowest mp (100°C). The trends in **Table 6** generally correspond with the average mps of the **Fxx**[43] and **Mxx**[45] series as well as the **Brxx** series[68] where five isomorphous pairs of **Clxx**/**Brxx**[68] are noted to have similar melting points (and within a range of 10-15°C). The highest mp usually corresponds to a *para-para* (**pp**) isomer and the lowest typically from one of the *ortho-meta*/*meta-ortho* (**om**/**mo**) pairs.[43] The **Clxp** triad has, on average, higher mps than **Clxm** or **Clxo**. For the corresponding analysis, the **Clpx** triad has the highest average compared to **Clmx** and **Clox**. Differences can be attributed to subtle and distinct secondary interactions that arise in the **Clxx**/**Brxx** pairs and their effect on melting points.

Table 6: Melting point averages for **Clxx** isomer grid.

Clxx isomers	Clpx	Clmx	Clox
***para* (Clxp)**	207♦	187	169
***meta* (Clxm)**	151	113#	136
***ortho* (Clxo)**	133	100*	136

Footnote: **Clpp** has the highest mp♦; **Clom** the lowest mp*, **Clmm** is a hydrate, **Clpo** is **Clpo_O**

The **Clxx** melting point ranges (**Table 6**) exhibit distinct differences when compared with their fluorine (**Fxx**)[43] and methylbenzamide analogues (**Mxx**), (ESI, Table S3).[45] The **Clxx** melting point ranges are on average ~20°C higher than the equivalent fluorinated **Fxx** systems (ESI; Figure S2, Table S3), with an average(± standard deviation) mp for the nine **Clxx** isomers of 148±34°C compared with 131°C for **Fxx**.[43] Moreover, the average mp for the **Brxx** series (147°C)[68] is similar to **Clxx**. This is not surprising given that five of the **Clxx** and **Brxx**[68] structures are isomorphous pairs with melting points within 10-15°C of each other. These values differ considerably from the average mps for the **Mxx**,[45] **NxxF**[44] and **NxxM**[46] series (ESI, Table S3) with average values of 116°C, 117°C and 113°C, respectively. The distinct differences stem from the chloro, fluoro and methyl substitution in **Clxx**, **Fxx**, **Mxx** and the reversed amide bridge for their **NxxF** and **NxxM** analogues. The question arises as to why differences arise between related series of isomer grids? All other things being equal, the effect of chlorine substitution in **Clxx** compared to fluorine or methyl is to bestow an average higher mp of 17°C compared to **Fxx**, which is 15°C greater than **Mxx** (as Br≈Cl>F>Me). The **Clxx**, **Fxx**, **Mxx** series have higher average melting points than their corresponding amide bridge reversed **NxxCl** (134°C), **NxxF** (117°C) and **NxxM** (113°C) isomer grids.[43-46]

In analysis of series of isomers and related congeners, it is important to be able to examine related structures and their physicochemical properties.[40-42,69-72,90-94] The CSD as a repository for structural information is important for ancillary information such as melting points.[40-42,90-94] In designing series of compounds, the drive to obtain a high melting point isomer should be influenced by the choice of Cl or Br-derivatives over F or Me and with *para*-substitutions where possible. Conversely, methyl-substituted and *meta*- or *ortho*-substituted are preferred for lower melting point compounds.[40-46,81-89]

Physicochemical and melting point relations

In order to try to relate the melting point temperatures to energies, additional analyses were conducted to identify correlations and trends.[58-62] The variation in the Gibbs free energy involves changes in enthalpy (ΔH) and entropy (ΔS): $\Delta G = \Delta H – T\Delta S$. At the melting point T_m, the system is in equilibrium so that the free energy of the melting equals zero ($\Delta G_f = 0$),[86] and the following equation holds:

$$T_m = \Delta H_m/\Delta S_m \qquad \text{(equation 1)}$$

Consequently, enthalpy and entropy changes are both determining in the melting point temperatures. A larger enthalpy of melting leads to a higher temperature value. Here, the melting point temperatures T_m are shown together with the estimated lattice electrostatic energy (E_{lat}) of the compounds in the ESI (Figure S4). The **Clmm** monohydrate crystal structure is not included as it has a different chemical content; it has the largest electrostatic cohesive energy but a small T_m value.

Globally, it appears that the two quantities T_m and E_{lat} are only moderately correlated (correlation factor = 47%). The isomers with highest T_m tend however to have the largest negative E_{lat} values, as shown by the positive sign of the correlation between $-E_{lat}$ and T_m for the **Clxx** isomer grids. Assuming electrostatics play a significant role in the stabilization of the crystal structure, it can indeed be expected that the electrostatic lattice energy E_{lat} of the **Clxx** isomers relates to their melting enthalpy, and therefore to T_m from equation 1, as discussed hereafter.

The entropy change ΔS_m also contributes to the melting point temperature. This quantity is largely dependent on the arrangement of the constituent groups in the molecule and therefore to the increase in the number of different available states ($\Delta S_m > 0$) upon the phase transition from an organized crystal structure to a liquid state.[86] Hence, one can expect a molecule with a high degree of rotational symmetry to show a smaller increase in entropy and, as a result, an increased T_m temperature (equation 1). For *para*-substituted compounds, the rotational symmetry of the molecule is higher with respect to the more unsymmetrical *ortho*- and *meta*-substituted **Clxx** isomers.

In an attempt to model Carnelley's rule, the *ortho*-/*meta*-/*para*-position descriptor f is introduced (**Figure 11a**).[81-89] The f(Clxx) function, defined as:

$$f(\text{Clxy}) = g(\text{x}) + g(\text{y}) \qquad \text{(equation 2)}$$

with g(m) = g(o) = 0 and g(p)=1, takes values 0, 1 or 2 as resulting from addition of *ortho* = *meta* = 0, *para* = 1 contributions. This descriptor yields, alone, a correlation value of 0.82 with the melting temperature values (**Figure 11a**). It represents, in a rudimentary way, the differences in entropy changes due to the variations in the substituent moiety positions. The variable f(**Clxx**), defined to model Carnelley's rule is therefore anti-correlated with the entropy variation upon melting.

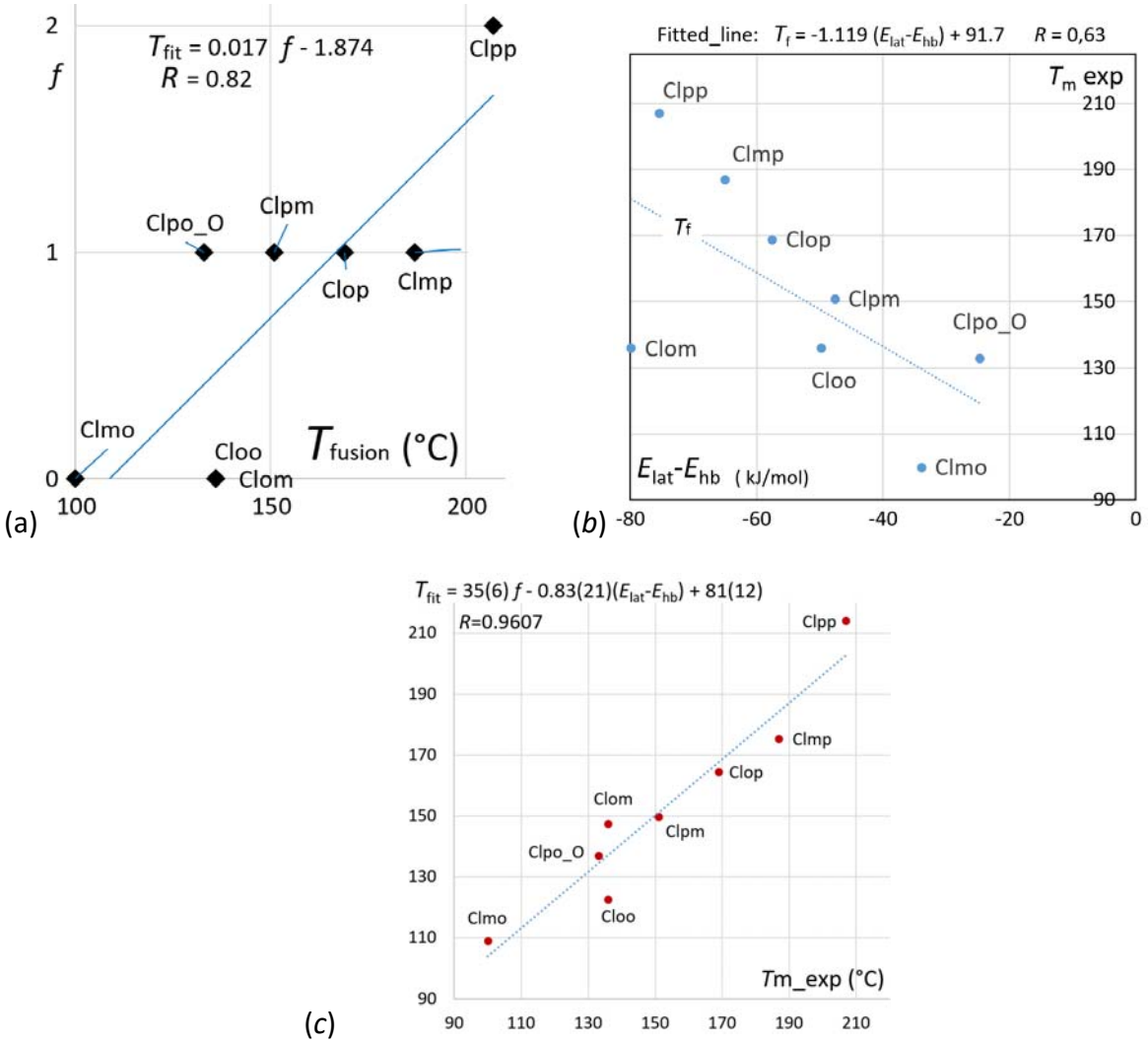

Figure 11. (*a*) Scatterplot of the experimental melting point T_m and and *f*(Clxx) symmetry descriptor. The *ortho-*/*meta-*/*para*-positions descriptor *f*(Clxy) is defined as *f*(Clxy) = *g*(x) + *g*(y), where *g*(m)=*g*(o)=0 and *g*(p)=1). The line shows the linear fit of the two variables T_m and *f*. (*b*) Scatterplot of T_m and (E_{lat}–E_{HB}), where E_{lat} is the lattice electrostatic energy and E_{HB} is the electrostatic energy between the two atoms involved in the strong hydrogen bond (N…H_N or O…H_N) atoms using the transferred multipolar atom model. (*c*) Double linear fit of melting point using the *f* and E_{lat}–E_{HB} parameters.

A double linear regression to fit T_m against the Carnelley *f* function values and E_{lat} set of variables leads to a correlation of 0.957 (ESI, Figure S5). This model has the advantage to account simultaneously for the enthalpic (through E_{lat}) and the entropic (through *f*) contributions to the melting temperature T_m.

The energetic contributions of strong N-H…N/O hydrogen bonds (E_{HB}) and the rest of interactions (E_{lat}-E_{HB}) were also evaluated. While the electrostatic energy between H_N and N/O atoms is on average -44 kJ.mol^{-1}, weaker C-H…O and C-H…N contacts have an energy lower than -20 kJ.mol^{-1}. The single fitting of T_m against E_{lat}-E_{HB} (correlation = -0.63 in **Table 7**, **Figure 11b**) is stronger than against E_{lat} (correlation factor = -0.47 in **Table 7** and Figure S4; ESI), suggesting that contributions to ΔH_m enthalpy are rather due to the weaker

interactions. Moreover, the non-existent dependence between T_m and E_{HB} (correlation factor = 0.09 in **Table 7**) also accounts for the same trend.

Comparison of the double linear regressions in Figure S5 (ESI) and **Figure 11c** further supports the evidence. Indeed, the 0.957 correlation found in Figure S5 (involving all electrostatic interactions) is only slightly lower than that described by the contributions of weaker interactions only (those excluding stronger HB's) in **Figure 11c**. The E_{HB} contribution in the former is compensated by the variation of the other fitting parameter f in the corresponding T_{fit} function.

Table 7. Linear correlation coefficients (%) (R) between several properties and variables.

Correlation	T_m	E_{lat}	f (Carnelley)	density	E_{HB}
E_{lat}	-47				
f (Carnelley)	83	45			
Crystal density	1	54	25		
E_{HB}	89	72	42	79	
E_{lat}-E_{HB}	-63	94	-14	30	44
Dipole μ [#]	26	-75	-2	79	-60

[#] The **Clxx** single molecule dipole moment

Accordingly, one can think that, at the melting point, weaker interactions will firstly dissociate because their intermolecular forces will not be able to restore their equilibrium solid-state geometries, while stronger interactions maintain their restoring forces. Overall, a high correlation such as presented herein (**Figure 11c**) might suggest a possible predictive behavior of the model, which will be further tested in studies of related series of **Yxx** substituted benzamides.[68]

The mean disagreement (as defined from the $|T_{fit}\text{-}T_m|/T_m$ value calculated over the eight data points) is respectively, <5.2% and <5.5% in the double linear regression fittings in **Figure 11c** and Figure S5 (ESI). The most important deviation (10%) is observed for **Cloo** in both fittings.

The lattice electrostatic energy E_{lat} was compared with E_{Syms}, the electrostatic interaction energy of the molecule with its immediate neighbouring molecules in the crystal packing (**Figure 12**). For all **Clxx** isomers, the E_{Syms} and E_{lat} values are very similar (**Figure 12a**), which shows that most of the lattice electrostatic energy originates from interactions with molecules directly in contact with the original molecule under study (*i.e*. the nearest neighbours). The energy values were computed for the four independent molecules (labelled as A=1, B=2, C=3, D=4) in the **Clmp** and **Clpm** crystal structures and averaged. The **Clpm** crystal structure is rather peculiar with molecules related by translation along the short unit cell axis a = 4.0095(4) Å which interact and result in an unfavourable electrostatic energy as electropositive/negative complementarity is not achieved. The E_{elec} values are all positive between dimers related by translation vector **a** in the **Clpm** crystal structure, +1.5, +1.8, +12.4 and +11.7 kJ.mol^{-1} for dimers 1 (A), 2 (B), 3 (C) and 4 (D), respectively.

For the 10 **Clxx** structures (including both **Clpo_O** and **Clpo_N** polymorphs, the hydrated **Clmm** and the averaged values for the four independent molecules in **Clmp** and **Clpm**), the

plotted E_{Syms} *vs* E_{lat} data (**Figure 12b**) are highly and linearly correlated. Indeed, the linear fitting between the two sets of values is E_{Syms} = 1.028(57) and E_{lat} + 0(6) (with a correlation factor R = 0.9877). The external disagreement (as defined by the fitting parameter of the slope) is lower than 3%, while the internal disagreement (as defined by the mean $|E_{Syms}–E_{lat}|/E_{lat}$) value calculated for the data) is 5%. The most important deviation in the internal disagreement is found for **Clmo** (14%).

The hydrogen bond contribution E_{HB} to the electrostatic energies were also computed as E_{elec} between H_N and N/O atoms) (ESI, Figure S9). The E_{HB} values are inversely correlated with the d(H_N…N/O) distances. The **Clom** structure has the strongest E_{lat} value, which is due to having both the strongest H_N…N hydrogen bond energy (shortest H_N…N of 1.894 Å, 2.073(17) Å and E_{lat}-E_{HB} complement. The longest N-H…N bond is noted in **Clmo**, with d(N,H_N)=2.302, 2.45(2) Å; it has the weakest E_{HB}; **Clmo** has two molecules related by an inversion centre to form a hydrogen bonded dimer as a cyclic $R^2_2(8)$ ring with two N-H…N interactions in close proximity.[43-46]

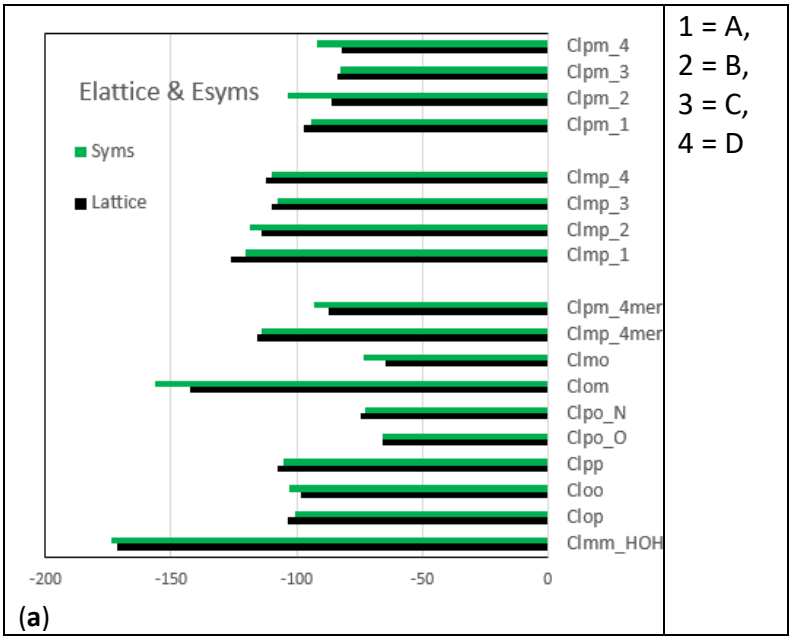

(**a**)

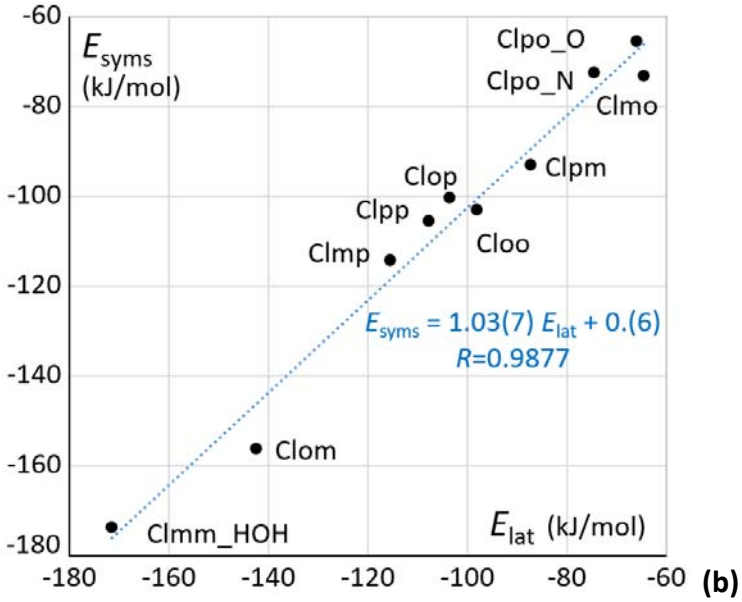

Figure 12. (**a**) A plot of E_{lat} (electrostatic lattice energy) and E_{Syms} (electrostatic interaction energy between a central molecule and its nearest neighbours) for the ten **Clxx** crystal structures. (**b**) Linear fitting of E_{syms} *vs*. E_{lat}. Energies are in kJ.mol^{-1}.

Other properties have also been analysed in the search for correlations that could be related to the melting temperature variations amongst the **Clxx** benzamides studied (**Table 7**). For instance, there is no correlation established between the mp temperature and the crystal density.

Contacts analysis

The intermolecular interactions of the isomer grid have been quantified using Hirshfeld surface analysis. The definition of enrichment ratios of contact has been detailed.[95-96] The enrichment ratio ε_{XY} for a pair of elements (X,Y) is defined as the ratio between the proportion of actual contacts in the crystal and the theoretical proportion of equi-distributed random contacts. An enrichment ratio larger than unity reveals that the contacts between a pair of elements are over-represented.

Table 8. Average % of intermolecular contacts C_{xy} and their enrichment ε_{xy} in the 9 non-hydrated **Clxx** structures. The standard deviations (*sd*) are in parentheses. The hydrophobic and hydrophilic groups are separated by lines. The ε_{XY}>>1 ratios are in **bold** and correspond to the significantly enriched contacts. H_N…H_N and O…H_N contacts have three large ε values and six small or zero values, therefore their standard deviations (*sd*'s) are large. The last row shows the average chemical content on the Hirshfeld surface.

C_{xy}	C	H_C	Cl	N	O	H_N
C	**13(3)**					
H_C	**29(6)**	**11(4)**			% contacts	
Cl	7(3)	**16(4)**	1(1)			
N	2.3(12)	4.4(18)	0.5(11)	0.1(1)		
O	3.1(13)	5.5(23)	0.5(12)	0.2(3)	0(0)	
H_N	0.6(6)	0.6(4)	0.2(4)	3.6(16)	1.1(17)	0.0(3)
C	1.2(3)					
H_C	1.0(3)	0.8(3)			enrichment	

Cl	0.8(3)	1.6(3)	0.6(7)			
N	0.7(3)	0.9(4)	0.3(7)	0.2(4)		
O	0.8(4)	**1.5(6)**	0.3(8)	0.3(6)	0.2(6)	
H_N	0.3(3)	0.3(2)	0.1(4)	**11(4)**	**2.7(48)**	1.9(27)
% surface	36.1	36.5	13.6	5.5	5.1	3.2

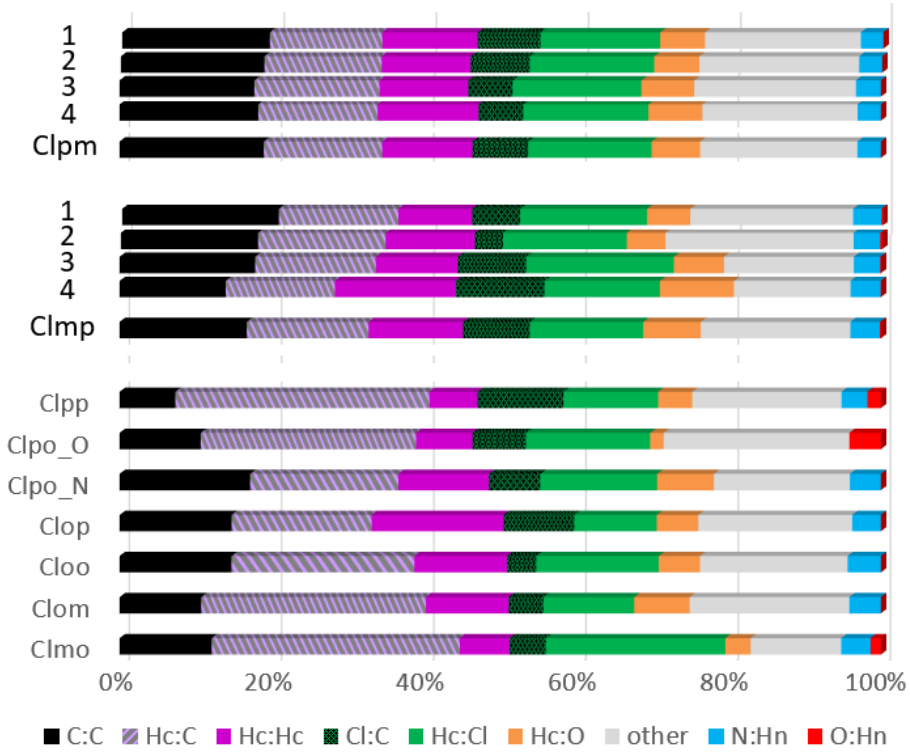

Figure 13. The % of contacts in the 9 non-hydrated **Clxx** crystal structures. The contacts of all four independent molecules in **Clmp** and **Clpm** crystal structures are depicted.

The average statistics on crystal contacts are listed in **Table 8**, while data on each individual crystal structure are presented (**Figure 13** and ESI, Table S4). The **Clxx** benzamide molecules are reasonably hydrophobic as the surface comprises just 14% of hydrophilic atoms (O, H_N, N). The contacts between hydrophobic atoms (C, H_C, Cl) account for 78% of the interaction surface while polar contacts involving only (H_N, O, N) atoms represent just 5% in the nine **Clxx** crystal structures. The cross contacts between hydrophobic and polar atoms constitute 17% of the surface and are mainly weak hydrogen bonds of C-H…O type (5.5%) and C-H…N (4.4%). All polar…non-polar cross interactions between atoms are, on average, under-represented, except the weak C-H…O hydrogen bonds. The partition between hydrophobic contacts (78±1)%, hydrophilic (5±1)% and cross contacts (17±2)% is quite stable in the nine non-hydrated **Clxx** isomers (ESI, Table S6).

Amongst all contacts in the nine **Clxx** non-hydrated crystals, the H_N…N strong hydrogen bond is on average the most enriched at ε = 11(4). The **Clpo_O** structure is the only one where the hydrogen bond donor N-H interacts strongly with the amide oxygen atom (as amide…amide interactions). The **Clpp** crystal structure is also peculiar, as both H_N…N and H_N…O are enriched (ε = 4.0 and 2.0) due to the presence of a bifurcated hydrogen bond (contact), with d(N…H_N) = 2.441(19) Å and d(O…H_N) = 2.837(17) Å. In the **Clmo** crystal

structure, a secondary long distance electrostatic interaction $d(H_N...O)$ = 3.266(18) Å also forms, in addition, to the primary $d(H_N...N)$= 2.45(2) Å hydrogen bond.[25-30,40-42]

All self contacts between charged atoms (O, N, H_N) are generally avoided as they are not favourable from an electrostatic viewpoint.[95,96] However, in the **Cloo** and **Clmo** crystal structures, the N-H and N acceptor atoms are in close proximity resulting in the formation of a double N-H…N hydrogen bond with graph set $R^2_2(8)$ (around a two-fold axis and inversion centre, respectively) leading to secondary $H_N...H_N$ contacts.[43-46]

The vast majority of intermolecular interactions are hydrophobic in nature, they constitute the five most represented contacts and four of them have C_{xy} proportions larger than 11%. The $Cl^{\delta-}...H_C^{\delta+}$ contact is the most enriched between the hydrophobic atom types and is considered as a weak hydrogen bond.[25-30] It is slightly attractive from an electrostatic point of view; for example the Cl3…H13 contact in **Clmp** (x-1,y,z+1, d = 3.00 Å) yields an energy between the two multipolar atoms of -2.4 kJ.mol^{-1}. The H_C…Cl contact is, on average, the only enriched contact formed by chlorine in the **Clxx** series. H_C has been noted to be a favoured partner for organic halogen atoms in several families of molecules.[96] The O…Cl and N…Cl contacts are, on average, quite disfavoured (with $\langle\mathcal{E}\rangle$ = 0.3) with halogen bonding absent in all but one structure.[31-39] **Clop** exhibits a typical Cl…O halogen bond with d(O,Cl) = 3.1104(18) Å and a C-Cl…O angle of 161.08(8)° which is not far from linearity (180°). The electrostatic energy between Cl and O atoms is however, slightly positive (unfavourable) at 1.5 kJ.mol^{-1}. In two other crystal structures, these contacts do occur and leading to enrichment values larger than unity. The **Cloo** structure has three long range Cl…N contacts, while **Clmm•H$_2$O** has several long Cl…O and Cl…N contacts.[31-39] The Cl…Cl contacts have on average an enrichment equal to unity but they only occur in half of the **Clxx** crystal structures. A significantly enriched and short Cl…Cl contact occurs only in the **Clom** structure (ESI, Figure S10).[31-39]

In the **Clxx** benzamides the C…C contacts are slightly enriched due to the occurrence of aromatic donor…acceptor interactions between aromatic rings.[30] Two aromatic rings with the $Cl^{\delta-}$ and $N^{\delta-}$ atoms have the ability to form favorable stacking interactions. Heterocycles have a good propensity to form ring stacking as the electropositive and electronegative atoms can be interacting partners.[97] For example in the **Cloo** and **Clom** structures, the N-C_5NH_4 group is in a parallel displaced interaction with symmetry related rings through an inversion center and the N atoms are located in opposite directions. In **Clpo_N**, the entire O=C-(NH)C_5H_4N moiety is in a parallel stacking mode with itself through an inversion center. In **Clop**, the same self-interaction occurs and in addition the pyridine ring forms a cross interaction with the chlorobenzene ring of a symmetry related **Clop** molecule. The **Clmm•H$_2$O** crystal structure has the highest $\mathcal{E}_{CC}$ = 2.0 ratio and shows extensive aromatic ring stacking in the *a*-axis direction of the whole (nearly planar) benzamide molecule with symmetry-related rings through an inversion center. This occurs in the **Clmp** crystal (Z'=4) as well, where stacking along the *c*-axis occurs through an alternation of crystallographic inversion and non-crystallographic pseudo-inversion symmetry operations. The **Clpm** crystal is unusual as the four independent molecules (A−D) show parallel displaced stacking through a translation (and not an inversion) along the short axes (a = 4.01 Å). Consequently, this **Clpm** crystal structure exhibits unusually enriched O…O and Cl…Cl contacts.[31-39]

The linear correlation coefficient *R* between the enrichment ratios found in the nine **Clxx** non-hydrate crystals is displayed in Table S7 (ESI). As a reference, a set of 9 random variables taking values in the [0,1] interval, yields a root mean square rms(*R*) value of 0.35. For further reference, rms(*R*) is 0.40 and the average is <*R*> = -0.05 for the enrichment ratios in **Clxx**. However, a few correlations take significant values up to 0.96, in terms of absolute value. Very large correlations should have a chemical meaning while moderate values may be explained or may be incidental due to limited sample size. The analysis highlights some clear trends but also shows some absence of correlations.

The two strong hydrogen bonds O…H_N and N…H_N are inversely-correlated, as could be expected (with *r* = -0.45). The strong and weak hydrogen bonds N…H_N and N…H_C turn out to be the most anti-correlated contacts (with *R* = -0.96), as all **Clxx** crystals, except for **Clpo_O**, have a N-H…N hydrogen bond. Conversely, the O…H_N and O…H_C which are both mildly enriched, on average, occur in an unrelated way in the crystal packings (with *R* = 0.07). Among the hydrophobic contacts, the $\mathcal{E}_{CC}$ and $\mathcal{E}_{CHc}$ values are 56% correlated while the $\mathcal{E}_{CC}$ and $\mathcal{E}_{HcHc}$ values display an *R* value of -50%. The correlation *R* = 0.79 between $\mathcal{E}_{CC}$ and $\mathcal{E}_{NN}$ may be explained by the concomitant occurrence of stacking between the pyridine heterocycles.

Conclusions

A series of nine **Clxx** benzamide isomers have been analysed for comparisons and show a degree of correlation with the related **Fxx**, **Mxx** benzamides,[43,45] and especially with **Brxx**[68] in terms of isomorphous behaviour.[90-94] In terms of their physicochemical behaviour, the series builds on our knowledge of isomeric relationships and shows that **Clxx** and **Brxx** behave largely in a similar fashion and differing substantially from the **Fxx** and **Mxx** isomer grids. The **Clxx** series provides examples such as the **Clpp** isomorphous/isostructural relationship with several **Xpp** relatives[43-46] and considerable overlap between **Clxx** and **Brxx** (with five isomorphous pairs), though much less so with **Fxx** and **Mxx**. Both can be rationalised as being influenced by strong hydrogen bonding dominating the interactions in solution and at the crystallization event, with the halogens having similar (Br, Cl) and different (Cl, F) steric and electronic influences on intermolecular interactions.[31-39] Our results indicate the dominance of N-H…N over N-H…O=C interactions in **Yxx** work[43-46,68] The transition from Me to F to Cl to Br shows the differences between the role of switching F/H position (steric/electronic) to structures where replacement by Cl or Br shows increasing crystal structure overlap,[34] and where the effect of the halogen on structure and interactions is more noteable.

Within the **Clxx** grid, examples include the two **Clpo** polymorphs which crystallise in the same space group (*Z*'=1) which is relatively rare though not unusual.[40-42,78] The **Clpo_N** crystal structure crystallises with lattice voids of dimensions similar in size to H_2 molecules. Of interest is the preponderance of *para-meta* substituted (**pm**) crystal structures observed with *Z*'=4 in the Cl, F, Me series of compounds studied to date, including **Clpm** and **Clmp** from this study. However, the **Brxx** and **NxxBr** series[68] do not contain any crystal structures with *Z*'>2.[73,75] Of note is that there is a lack of Cl…O and Cl…N halogen bonding interactions in **Clxx** apart from the **Clpp**, **Clop** and **Clom** structures.[31-39] This can be attributed to the fact that there is only one halogen atom (Cl) per molecule and there is considerable competition with other interactions. The pyridine N atom is rather involved in the formation of strong

hydrogen bonds with H-N, while the amide O atom generally forms weaker C-H…O hydrogen bonds. On the other hand, the C-H…Cl weak hydrogen bonds have a more favourable electrostatic energy than the Cl…O/N halogen bonding.[31-39]

The **Clxx** isomer grid provides an illustration of Carnelley's rule, which relates the crystal melting temperature to the symmetry of the crystallized molecule.[81-89] An empirical function based on the substituent positions and the lattice electrostatic energy is introduced, allowing us to obtain the fitted melting temperatures which are more than 95% correlated with the experimental values. Given the high correlation, this model will be further refined in series of related benzamides and its possible predictive behaviour will be evaluated.

The entropic component of T_m has been related to molecular symmetry using the *f*-descriptor, which accounts for the *ortho*-/*meta*-/*para*-positions differentiating the local symmetry of the **Clxx** molecular structures. On the other hand, from an investigation of simple fittings of the melting point T_m, it demonstrates that the one based on E_{lat}-E_{HB} accounts for a better correlation than from the total lattice electrostatic energy E_{lat}. This trend suggests that the enthalpic component of T_m is better described by weaker solid-state interactions. When a double linear regression of T_m against either (E_{lat}-E_{HB}, *f*) or (E_{lat}, *f*) is carried out, a similar good correlation is however, obtained in both cases, because the fitting parameters absorb the electrostatic contribution of stronger HB's that are included in E_{lat}. Hence, any of the T_{fit} models could be used in the prediction of melting points for related series of **Yxx** substituted benzamides.[43-46,68]

Similar melting points were found for the **Clxx** and **Brxx** series,[68] which exhibit five isomorphous pairs with T_m values within 10-15°C of each other. This suggests that the ΔH_m component of T_m could be strongly dependent on the relative orientations of molecules found in the molecular assembly that forms the solid-state. Indeed as related **Clxx** and **Brxx**[68] pairs exhibit the same molecular symmetry, the ΔS_m entropic component is expected to be comparable. Similar T_m values are thus pointing towards similar ΔH_m values in the isomorphous structures. The related pairs in the **Clxx** and **Brxx** series are built by equivalent molecular packing and molecular orientations in their assemblies. This trend could be brought close to the previous indications on the enthalpic contributions to T_m, is mainly driven by the weaker interactions rather than by the intensity difference of stronger interactions.

The Hirshfeld surface analysis shows that the strong hydrogen bond O…H_N (or O…H_N in **Clpo_O**) is the most enriched contact type followed by the weak hydrogen bonds Cl…H_C and O…H_C. Hydrophobic atoms (C, H_C, Cl) generally prefer to interact within their subgroup with the exception of the over-represented O…H_C contacts.

In conclusion, the N-H…N intermolecular interaction type dominates in **Clxx**, and largely in the absence of solvates and the Cl atoms only engage in weak C-H…Cl hydrogen bonds. Five of the **Clxx** form isomorphous pairs with their **Brxx** analogues and with **Clpp** isomorphous with several close benzamide relatives. Analysis of the melting point temperatures T_m reveals correlations involving both molecular symmetry and electrostatic energies. In future work, the structural and physicochemical aspects of the amide bridge reversed **NxxCl** series and bromo-containing derivatives (**Brxx**, **NxxBr**) will be reported as well as an overview of

the halogenated benzamide research.[43-46,68] This **Yxx** research will be placed in context in light of on-going developments in related areas.[43-46,68,98] Expanding the domain of X-ray crystallography in combination with theoretical calculations will enhance our knowledge and understanding of the physicochemical properties of molecular systems.[98]

Supplementary Information

Crystallographic data for the ten **ClxxC** crystal structures have been deposited with the Cambridge Crystallographic Data Centre, CCDC no. 1878555 to 1878564. CIF data may be downloaded from the CCDC website https://summary.ccdc.cam.ac.uk/structure-summary-form or obtained free of charge from The Director, CCDC, 12 Union road, Cambridge, CB2 1EZ, U.K. (fax: +44-1223-336033; e-mail: deposit@ccdc.cam.ac.uk). The structural data are available as CIF files from the corresponding author Professor John F. Gallagher (DCU).

Acknowledgements

This research was part-funded by the Programme for Research in Third Level Institutions (PRTLI) Cycle 4 (Ireland) and co-funded through the European Regional Development Fund (ERDF), part of the European Union Structural Funds Programme (ESF). The Irish Centre for High End Computing (ICHEC) is thanked for computer resource allocation, support and assistance with the computational calculations (http://www.ichec.ie). The authors warmly thank the Region Lorraine for a FEDER Chercheur d'Avenir grant (2015-2018).

References

(1) Gribble, G. W. Naturally Occuring Organohalogen Compounds — A Comprehensive Survey. *Prog. Chem. Org. Nat. Prod*. **1996**, *68*, 1–423.

(2) Gribble, G. W. Naturally occurring organohalogen compounds. *Acc. Chem. Res*. **1998**, ***31***, 141–152.

(3) Gribble, G. W. The diversity of naturally occurring organobromine compounds. *Chem. Soc. Rev*. **1999**, *28*, 335–346.

(4) Gribble, G. W. The diversity of naturally produced organohalogens. *Chemosphere* **2003**, *52*, 289–297.

(5) Gribble, G. W. Recently Discovered Naturally Occurring Heterocyclic Organohalogen Compounds. *Heterocycles*, **2012**, *84*, 157–207.

(6) Gribble, G. W. A recent survey of naturally occurring organohalogen compounds. *Environmental Chemistry* **2015**, *12*, 396–405.

(7) Müller, K.; Faeh, C.; Diederich, F. Fluorine in pharmaceuticals: Looking beyond intuition. *Science* **2007**, *317*, 1881−1886.

(8) Wang, J.; Sánchez-Roselló, M.; Aceña, J. L.; del Pozo, C.; Sorochinsky, A. E.; Fustero, S.; Soloshonok, V. A.; Liu, H. Fluorine in Pharmaceutical Industry: Fluorine-Containing Drugs Introduced to the Market in the Last Decade (2001-2011) *Chem. Rev*. **2014**, *114*, 2432–2506.

(9) Banks, R. E.; Smart, B. E.; Tatlow. J. C. Eds., *Organofluorine chemistry: Principles and Commercial Applications* **1994**, *11*, Springer Science.

(10) Jeschke, P. The unique role of halogen substituents in the design of modern agrochemicals. *Pest Manage. Sci*. **2010**, *66*, 10−27.

(11) Jeschke, P. Progress of modern agricultural chemistry and future prospects. *Pest Manage. Sci*. **2016**, *72*, 433–455.

(12) Jeschke, P. Latest generation of halogen-containing pesticides. *Pest Manage. Sci*. **2017**, *73*, 1053–1066.

(13) Yoder, N. C.; Kumar, K. Fluorinated amino acids in protein design and engineering. *Chem. Soc. Rev*. **2002**, *31*, 335−341.

(14) Luthe, G.; Swenson, D. C.; Robertson, L. W. Influence of fluoro-substitution on the planarity of 4-chlorobiphenyl (PCB 3). *Acta Crystallogr*. **2007**, *B63*, 319−327.

(15) Klösener, J.; Swenson, D. C.; Robertson, L. W.; Luthe, G. Effects of fluoro substitution on 4-bromodiphenylether (PBDE 3). *Acta Crystallogr*. **2008**, *B64*, 108−119.

(16) Babudri, F.; Farinola, G. M.; Naso, F.; Ragni, R. Fluorinated organic materials for electronic and optoelectronic applications: the role of the fluorine atom. *Chem. Commun.* **2007**, 1003−1022.

(17) Berger, R.; Resnati, G.; Metrangolo, P.; Weber, E.; Hulliger, J. Organic fluorine compounds: a great opportunity for enhanced materials properties. *Chem. Soc. Rev*. **2011**, *40*, 3496−3508.

(18) Marsh, E. N. G. Fluorinated Proteins: From Design and Synthesis to Structure and Stability. *Acc. Chem. Res*. **2014**, *47*, 2878−2886.

(19) Gillis, E. P.; Eastman, K. J.; Hill, M. D.; Donnelly, D. J.; Meanwell, N. A. Applications of Fluorine in Medicinal Chemistry. *J. Med. Chem*. **2015**, *58*, 8315−8359.

(20) Lehn, J.-M. *Supramolecular Chemistry: Concepts and Perspectives*, **1995**, VCH, Weinheim, Germany.

(21) Tiekink, E. R. T.; Vittal, J. J. *Frontiers in Crystal Engineering*, **2005**, Wiley.

(22) Desiraju, G. R.; Vittal, J. J.; Ramanan, A. *Crystal Engineering*, **2011**, World Scientific.

(23) Steed, J. W.; Gale, P. A. *Supramolecular Chemistry: from Molecules to Nanomaterials*, **2012**, *1-8*, Wiley, Hoboken, New Jersey, USA.
(24) Bürgi, H.-B.; Dunitz, J. D. *Structure Correlation*, **2008**, Volume 1, John Wiley and Sons Inc, Wiley Online Library. DOI: 10.1002/9783527616091
(25) Desiraju, G. R.; Steiner, T. *The weak hydrogen bond in structural chemistry and biology*, **2001**, Oxford University Press, UK.
(26) Domenicano, A.; Hargittai, I. *Strength from Weakness: Structural Consequences of Weak Interactions in Molecules, Supermolecules and Crystals*, **2002**, *68*, NATO Science series II, Springer Netherlands.
(27) Nishio, M. CH/π hydrogen bonds in crystals. *CrystEngComm.* **2004**, *6*, 130−158.
(28) Dance, I.; Scudder, M. Molecules embracing in Crystals. *CrystEngComm.* **2009**, *11*, 2233−2247.
(29) Alvarez, S. A cartography of the van der Waals territories. *Dalton Trans*. **2013**, *42*, 8617−8636.
(30) Martinez, C. R.; Iverson, B. L. Rethinking the term "pi-stacking". *Chem. Sci*. **2012**, *3*, 2191–2201.
(31) Metrangolo, P.; Resnati, G. Eds., *Halogen Bonding: Fundamentals and Applications; Structure and Bonding*, Springer, Berlin, **2008**, *126*.
(32) Raatikainen, K.; Rissanen, K. Breathing molecular crystals: halogen- and hydrogen-bonded porous molecular crystals with solvent induced adaptation of the nanosized channels. *Chem. Sci*. **2012**, *3*, 1235–1239.
(33) Desiraju, G. R.; Ho, P. S.; Kloo, L.; Legon, A. C.; Marquardt, R.; Metrangolo, P.; Politzer, P.; Resnati, G.; Rissanen, K. Definition of the halogen bond (IUPAC Recommendations 2013). *Pure Appl. Chem*. **2013**, *85*, 1711–1713.
(34) Mukherjee, A.; Desiraju, G. R. Halogen bonds in some dihalogenated phenols: applications to crystal engineering. *IUCrJ* **2014**, *1*, 49–60.
(35) Makhothkina, O.; Lieffrig, J.; Jeannin, O.; Fourmigué, M.; Aubert, E.; Espinosa, E. Cocrystal or Salt: Solid State-Controlled Iodine Shift in Crystalline Halogen-Bonded Systems. *Cryst. Growth Des*. **2015**, *15*, 3464–3473.
(36) Bauza, A.; Mooibroek, T. J.; Frontera, A. The Bright Future of Unconventional σ/π-Hole Interactions. *ChemPhysChem* **2015**, *16*, 2496–2517.
(37) Cavallo, G.; Metrangolo, P.; Milani, R.; Pilati, T.; Priimagi, A.; Resnati, G.; Terraneo, G. A. F. *Chem. Rev.* **2016**, *116*, 2476−2601.
(38) Kolar, M. H.; Hobza, P. Computer Modeling of Halogen Bonds and Other sigma-Hole Interactions. *Chem. Rev*. **2016**, *116*, 5155−5187.
(39) Tepper, R.; Schubert, U. S. Halogen Bonding in Solution: Anion Recognition, Templated Self-Assembly, and Organocatalysis *Angew. Chem.* Int. Ed. Engl. **2018**, *57*, 6004−6016.
(40) Allen, F. H. The Cambridge Structural Database: a quarter of a million crystal structures and rising. *Acta Crystallogr*. **2002**, *B58*, 380−388.
(41) Thomas, I. R.; Bruno, I. J.; Cole, J. C.; Macrae, C. F.; Pidcock, E.; Wood, P. A. WebCSD: the online portal to the Cambridge Structural Database. *J. Appl. Cryst*. **2010**, *43*, 362−366.
(42) Groom, C. R.; Bruno, I. J.; Lightfoot, M. P.; Ward, S. C. The Cambridge Structural Database. *Acta Crystallogr.* **2016**, *B72*, 171−179.
(43) Mocilac, P.; Donnelly, K.; Gallagher, J. F. Structural systematics and conformational analyses of a 3×3 isomer grid of fluoro-N-(pyridyl)benzamides: physicochemical

correlations, polymorphism and isomorphous relationships. *Acta Crystallogr*. **2012**, *B68*, 189−203.
(44) Mocilac, P.; Lough, A. J.; Gallagher, J. F. Structures and conformational analysis of a 3×3 isomer grid of nine N-(fluorophenyl)pyridinecarboxamides. *CrystEngComm* **2011**, *13*, 1899−1909.
(45) Mocilac, P.; Tallon, M.; Lough, A. J.; Gallagher, J. F. Synthesis, structural and conformational analysis of a 3×3 isomer grid based on nine methyl-N-(pyridyl)benzamides. *CrystEngComm* **2010**, *12*, 3080−3090.
(46) Mocilac, P.; Gallagher, J. F. Structural systematics and conformational analyses of a 3×3 isomer grid of nine N-(tolyl)pyridinecarboxamides and three chlorinated relatives. *CrystEngComm* **2011**, *13*, 5354−5366.
(47) Mocilac, P.; Gallagher, J. F. Trezimides and Tennimides: New Imide-Based Macrocycles. *J. Org. Chem*. **2013**, *78*, 2355−2361.
(48) Mocilac, P.; Gallagher, J. F. Halogen bonding directed supramolecular assembly in bromo-substituted trezimides and tennimides. *CrystEngComm* **2014**, *16*, 1893−1903.
(49) Mocilac, P.; Gallagher, J. F. Halogenated tennimides and trezimides: impact of halogen bonding and solvent role on porous network formation and inclusion. *CrystEngComm* **2016**, *18*, 2375−2384.
(50) Oxford Diffraction Ltd ABSFAC and CrysAlisPro CCD/RED *Version 1.171.33.55* Oxford Diffraction, Abingdon, Oxon, UK.
(51) Sheldrick, G. M. A short history of SHELX. *Acta Crystallogr.* **2008,** *A64*, 112−122.
(52) McArdle, P. SORTX - a program for on-screen stick-model editing and autosorting of SHELX files for use on a PC. *J. Appl. Cryst*. **1995**, *28*, 65−65.
(53) Spek, A. L. Single-crystal structure validation with the program PLATON. *J. Appl. Cryst*. **2003**, *36*, 7−13.
(54) Macrae, C. F.; Edgington, P. R.; McCabe, P.; Pidcock, E.; Shields, G. R.; Taylor, R.; Towler, M.; van de Streek, J. Mercury: visualization and analysis of crystal structures. *J. Appl. Cryst.* **2006**, *39*, 453−457.
(55) Frisch, M. J. *et al*., Gaussian 09 *Revision B.01,* **2010**, Gaussian Inc. Wallingford CT USA.
(56) Becke, A. D. Density-Functional Thermochemistry. 3. The Role of Exact Exchange. *J. Chem. Phys.* **1993**, *98*, 5648−5652.
(57) Krishnan, R.; Binkley, J. S.; Seeger, R.; Pople, J. A. Self-Consistent Molecular-Orbital Methods. 20. Basis Set For Correlated Wave-Functions. *J. Chem. Phys*. **1980**, *72*, 650−654.
(58) Jelsch, C.; Guillot, B.; Lagoutte, A.; Lecomte, C. Advances in protein and small-molecule charge-density refinement methods using MoPro. *J. Appl. Cryst*. **2005**, *38*, 38−54.
(59) Domagała, S.; Fournier, B.; Liebschner, D.; Guillot, B.; Jelsch, C. An improved experimental databank of transferable multipolar atom models-ELMAM2. Construction details and applications. *Acta Crystallogr*. **2012**, *A68*, 337−351.
(60) Allen, F. H.; Bruno, I. J. Bond lengths in organic and metal-organic compounds revisited: X-H bond lengths from neutron diffraction data. *Acta Crystallogr*. **2010**, *B66*, 380−386.
(61) Guillot, B.; Espinosa, E.; Huder, L.; Jelsch, C. MoProViewer: a tool to study proteins from a charge density science perspective. *Acta Crystallogr*. **2014**, *A70*, C279.

(62) Jelsch, C.; Bisseyou, Y. B. M. Atom interaction propensities of oxygenated chemical functions in crystal packings. *IUCrJ* **2017**, *4*, 158–174.
(63) Mocilac, P.; Gallagher, J. F. The First Phenyl-N-pyridinylcarbamate Structures: Structural and Conformational Analysis of Nine Methoxyphenyl-N-pyridinylcarbamates. *Cryst. Growth Des.* **2013**, *13*, 5295–5304.
(64) Mocilac, P.; Gallagher, J. F. Structural systematics and conformational analyses of an isomer grid of nine tolyl-N-pyridinylcarbamates. *Structural Chemistry,* **2017**, *28*, 697–708.
(65) Noveron, J. C.; Lah, M. S.; Del Sesto, R. E.; Arif, A. M.; Miller, J. S.; Stang, P. J. Engineering the structure and magnetic properties of crystalline solids via the metal-directed self-assembly of a versatile molecular building unit. *J. Am. Chem. Soc.* **2002**, *124*, 6613−6625.
(66) Donnelly, K.; Gallagher, J. F.; Lough, A. J. Assembling an isomer grid: the isomorphous 4-, 3- and 2-fluoro-*N*'-(4-pyridyl)benzamides. *Acta Crystallogr*. **2008**, *C64*, o335−o340.
(67) McMahon, J.; Anderson, F. P.; Gallagher, J. F.; Lough, A. J. A structural systematic study of three isomers of difluoro-*N*-(4-pyridyl)-benzamide. *Acta Crystallogr*. **2008**, *C64*, o493−o497.
(68) Hehir, N. Structural systematics of halogenated benzamides. Dublin City University, Ireland. PhD thesis, **2017**.
(69) Bombicz, P. The way from isostructurality to polymorphism. Where are the borders? The role of supramolecular interactions and crystal symmetries. *Crystallography Reviews* **2017**, *23*, 118−151.
(70) Palma, A. Gallagher, J. F.; Muller-Bunz, H.; Wolowska, J.; McInnes, E. J. L.; O'Shea, D. F. Co(II), Ni(II), Cu(II) and Zn(II) complexes of tetraphenylazadipyrromethene. *Dalton Trans*. **2009**, 273−279.
(71) Gelbrich, T.; Hursthouse, M. B.; Threlfall, T. L. Structural systematics of 4,4'-disubstituted benzenesulfonamidobenzenes. 1. Overview and dimer based isostructures. *Acta Crystallogr*. **2008**, *B63*, 621−632.
(72) Gelbrich T.; Threlfall, T. L. The crystal structure of methyl paraben at 118 K does not represent a new polymorph. *Cryst. Growth Des*. **2007**, *7*, 2297−2297.
(73) Brock, C. P. High-*Z*' structures of organic molecules: their diversity and organizing principles. *Acta Crystallogr.* **2016**, *B72*, 807−821.
(74) Das, U.; Chattopadhyay, B.; Hazra, D. K.; Sureshbabu, V. V.; Mukherjee, A. K. Two carbamate derivatives with *Z*'=2 and 3: An interplay of strong and weak hydrogen bonds. *J. Mol. Struct*. **2016**, *1122*, 290−298.
(75) Steed, K. M.; Steed, J. W. Packing Problems: High *Z*′ Crystal Structures and Their Relationship to Cocrystals, Inclusion Compounds, and Polymorphism. *Chem. Rev*. **2015**, *115*, 2895−2933.
(76) Brittain, H. G. Ed. *Polymorphism in Pharmaceutical Solids*, **1999**, 1st Ed. New York: Marcel Dekker Inc.
(77) Bernstein, J. *Polymorphism in Molecular Crystals*, **2002**, Oxford: Clarendon Press.
(78) Yu, L. Polymorphism in Molecular Solids: An Extraordinary System of Red, Orange, and Yellow Crystals. *Acc. Chem. Res*. **2010**, *43*, 1257−1266.
(79) Brittain, H. G. Polymorphism and solvatomorphism 2010. *J. Pharm. Sci.* **2012**, *101*, 464−484.

(80) Steed, J. W. Understanding exceptional polymorphs. *Acta Crystallogr*. **2016**, *B72*, 805−806.
(81) Abramowitz, R.; Yalkowsky, S. H. MELTING-POINT, BOILING-POINT, AND SYMMETRY, *Pharm. Res*. **1990**, *7*, 942−947.
(82) Brown, R. J. C.; Brown, R. F. C. Melting point and molecular symmetry. *J. Chem. Ed.* **2000**, *77*, 724−731.
(83) Vishweshwar, P.; Nangia, A.; Lynch, V. M. Molecular complexes of homologous alkanedicarboxylic acids with isonicotinamide: X-ray crystal structures, hydrogen bond synthons, and melting point alternation. *Cryst. Growth Des*. **2003**, *3*, 783−790.
(84) Slovokhotov, Y. L.; Neretin, I. S.; Howard, J. A. K. Symmetry of van der Waals molecular shape and melting points of organic compounds. *New J. Chem*. **2004**, *28*, 967−979.
(85) Podsiadło, M.; Bujak, M.; Katrusiak, A. Chemistry of density: extension and structural origin of Carnelley's rule in chloroethanes. *CrystEngComm* **2012**, *14*, 4496−4500.
(86) Yalkowsky, S. H. Carnelley's Rule and the Prediction of Melting Point. *J. Pharm. Sci*. **2014**, *103*, 2629−2634.
(87) Gamidi, R. K.; Rasmuson, A. Estimation of Melting Temperature of Molecular Cocrystals Using Artificial Neural Network Model. *Cryst. Growth Des*. **2017**, *17*, 175−182.
(88) Bujak, M. Melting point, molecular symmetry and aggregation of tetrachlorobenzene isomers: the role at halogen bonding. *Acta Crystallogr*. **2018**, *B74*, 458–466.
(89) Mishra, M. K.; Kelley, S. P.; Shamshina, J. L.; Choudhary, H.; Rogers, R. D. Can Melting Point Trends Help Us Develop New Tools To Control the Crystal Packing of Weakly Interacting Ions? *Cryst. Growth Des*. **2018**, *18*, 597−601.
(90) Abad, A.; Agullo, C.; Cunat, A. C.; Vilanova, C.; de Arellano, M. C. R. X-ray structure of fluorinated N-(2-chloropyridin-4-yl)-*N*'-phenylureas. Role of F substitution in the crystal packing. *Cryst. Growth Des*. **2006**, *6*, 46–57.
(91) Tuchalski, G.; Emmerling, F.; Groger, K.; Hansicke, A.; Nagel, T.; Reck, G. X-ray investigations of nebivolol and its isomers. *J. Mol. Struct*. **2006**, *800*, 28–44.
(92) Capacci-Daniel, C.; Dehghan, S.; Wurster, V. M.; Basile, J. A.; Hiremath, R.; Sarjeant, A. A.; Swift, J. A. Halogen/methyl exchange in a series of isostructural 1,3-bis(m-dihalophenyl) ureas. *CrystEngComm* **2008**, *10*, 1875−1880.
(93) Dumitru, F.; Legrand, Y. -M.; Barboiu, M.; van der Lee, A. Weak intermolecular hydrogen and halogen interactions in an isomorphous halogen series of pseudoterpyridine Zn-II complexes. *Acta Crystallogr*. **2013**, *B69*, 43−54.
(94) Gomes, L. R.; Low, J. N.; Cagide, F.; Borges, F. The crystal structures of four *N*-(4-halophenyl)-4-oxo-4H-chromene-3-carboxamides. *Acta Crystallogr*. **2015**, *E71*, 88−93.
(95) Jelsch, C.; Ejsmont, C.; Huder, L. The enrichment ratio of atomic contacts in crystals, an indicator derived from the Hirshfeld surface analysis. *IUCrJ* **2014**, *1*, 119−128.
(96) Jelsch, C.; Soudani, S.; Ben Nasr, C. Likelihood of atom-atom contacts in crystal structures of halogenated organic compounds. *IUCrJ* **2015**, *2*, 327−340.
(97) Salonen, L. M.; Ellermann, M.; Diederich, F. Aromatic Rings in Chemical and Biological Recognition: Energetics and Structure. *Angew Chem. Int. Ed*. *Engl.* **2011**, *50*, 4808−4842.

(98) Kofoed, P. M.; Hoser, A. A.; Diness, F.; Capelli, S. C.; Madsen, A. Ø. X-ray diffraction data as a source of the vibrational free-energy contribution in polymorphic systems. *IUCrJ* **2019**, *6*, 558−571.

Graphical Abstract

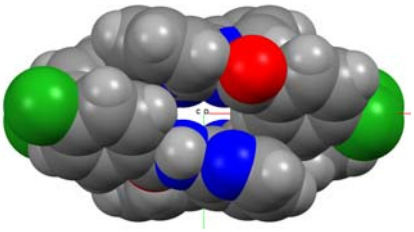

Physicochemical properties of a 3×3 isomer grid of mono-chlorobenzamides (**Clxx**) (**x** = *p*-/*m*-/*o*-) are reported. **Clpo** forms two polymorphs as **Clpo_N** (N-H…N interactions with void formation as depicted in the graphic) and **Clpo_O** (O-H…O interactions). Weak C-H…Cl hydrogen bonds are the only favoured interaction partner of Cl with halogen bonding mostly absent. The melting temperatures T_m have been correlated to both molecular symmetry and electrostatic energies.

ELECTRONIC SUPPLEMENTARY INFORMATION

At the interface of isomorphous behaviour in a 3×3 isomer grid of mono-chlorobenzamides: Analyses of the interaction landscapes *via* contact enrichment studies.

John F. Gallagher[*#], Mark Farrell, Pavle Mocilac, Niall Hehir

School of Chemical Sciences, Dublin City University, Dublin 9, Ireland

with

Emmanuel Aubert, Enrique Espinosa, Benoît Guillot, Christian Jelsch[*]

CRM[2], CNRS UMR 7036, Faculté des Sciences et Technologies, Université de Lorraine, BP 70239, Boulevard des Aiguillettes, 54506 Vandoeuvre-lès-Nancy, France

Corresponding author:[#]
Dr. John F. Gallagher,
School of Chemical Sciences,
Dublin City University, Dublin 9, Ireland
e-mail: john.gallagher@dcu.ie

TABLE OF CONTENTS:

CLASS OF COMPOUNDS STUDIED WITH DIAGRAMS SHOWING RING CONFORMATIONS:

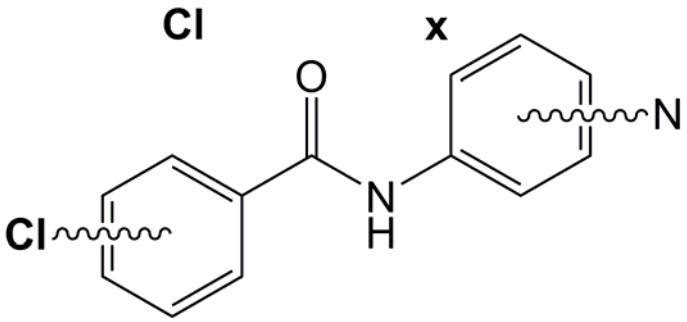

and

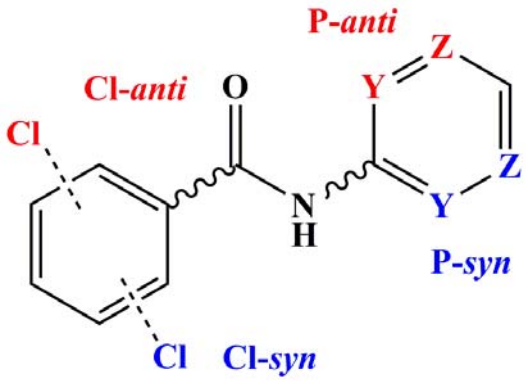

Figure S1. **Clxx** with the four general **Clxx** ring conformations.

Explanation of the Clxx nomenclature and relationship with NxxCl:
The 3×3 isomer grid of mono-chlorobenzamides (as **Clxx**) derive from the components with **Clx** = chlorobenzoyl or *para*-/*meta*-/*ortho*-ClC6H4C=O combined with **x** = *para*- or *meta*- or *ortho*-aminopyridine (HNC_5H_4N) substitutions. The related **NxxCl** series (next paper) is a series of 9 isomers related to **Clxx** but with a reversed amide bridge.

The **Fxx**,[43] **NxxF**,[44] **Mxx**[45] or **NxxM**[46] analogues of **Clxx**[present study] and **Brxx**[68]
The **Fxx** series is just a simple replacement of chlorine by fluorine and the **Mxx** series is likewise a replacement of chlorine by the methyl group. The **NxxF**[44] and **NxxM**[46] series are the amide bridged reversed isomers of **Fxx**[43] and **Mxx**[45] (although synthesised from different acyl chloride and amine starting materials).

Hpp[65] can be regarded as similar to **Fxx** and **Clxx** and as the parent compound for reference (and without any halide atom attached)

Figure S2. DIAGRAMS OF FIGURES REFERENCED IN THE TEXT.[43-46]

Representative examples of **Fxx** (with **Fpp** depicted below),[43] **Mxx** (**Mpp** depicted below),[45] **NxxF** (**NppF** depicted below)[44] and **NxxM** (**NppM** depicted below).[46]

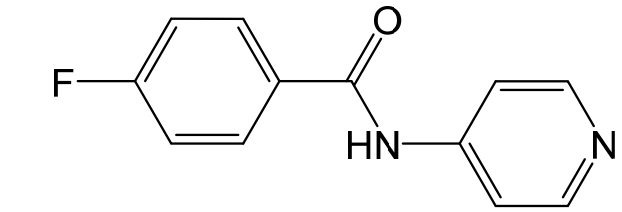

Fpp

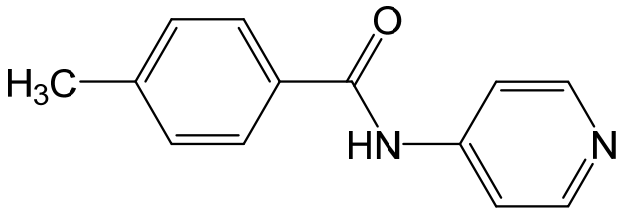

Mpp

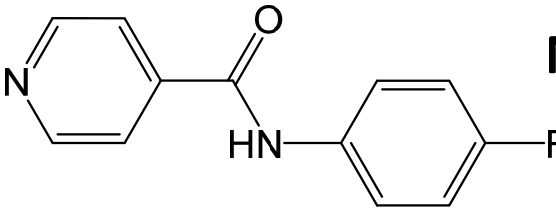

NppF

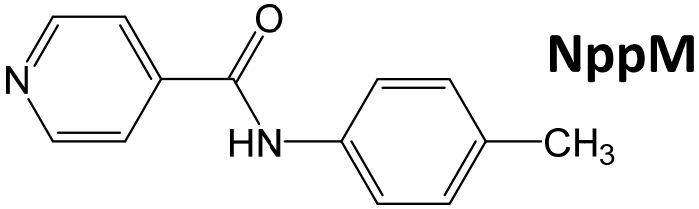

NppM

and

The difluorinated **25p** from reference 67.

A structural systematic study of three isomers of difluoro-N-(4-pyridyl)-benzamide. *Acta Crystallogr*. **2008**, *C64*, o493−o497.

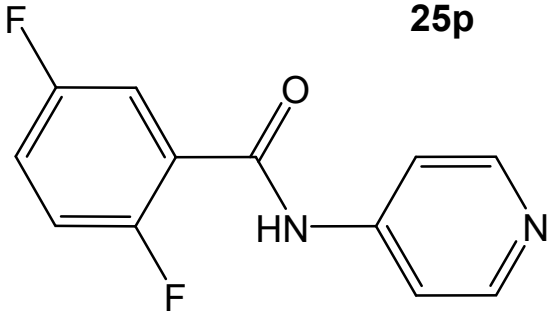

25p

TABLE S1. CRYSTAL STRUCTURE DATA: EXPERIMENTAL DETAILS

Experiments were carried out at 294 K using a Xcalibur, Sapphire3, Gemini Ultra. H atoms were treated by a mixture of independent and constrained refinement as CSD codes 1878555 to 1878564.

ClXX isomers	**ClPP**	**ClMP**	**ClOP**	**ClPM**	**ClMM_H_2O**
Crystal data					
Chemical formula	$C_{12}H_9ClN_2O$	$C_{12}H_9ClN_2O$	$C_{12}H_9ClN_2O$	$C_{12}H_9ClN_2O$	$C_{12}H_9ClN_2O{\cdot}H_2O$
M_r	232.66	232.66	232.66	232.66	250.68
Crystal system, space group	Monoclinic, $P2_1/c$	Triclinic, $P\bar{1}$	Orthorhombic, *Pbca*	Triclinic, $P\bar{1}$	Monoclinic, $P2_1/c$
a, *b*, *c* (Å)	5.6453(5), 11.7673(8), 16.2271(12)	11.4395(2), 12.9293(2), 14.8943(4)	9.3966(18), 12.0918(19), 19.295(4)	4.0095(4), 21.385(2), 27.378(3)	7.4273(5), 18.0819(10), 8.9461(6)
α, β, γ (°)	90, 96.791(7), 90	89.979(2), 76.924(2), 88.507(1)	90, 90, 90	112.717(9), 93.377(8), 92.305(8)	90, 107.948(7), 90
V (Å^3)	1070.40(14)	2145.05(8)	2192.4(7)	2156.6(4)	1142.99(13)
Z	4	8	8	8	4
Radiation type	Mo *K*α	Mo *K*α	Mo *K*α	Mo *K*α	Mo *K*α
μ (mm^{-1})	0.33	0.33	0.33	0.33	0.32
Crystal shape	Block	Block	Block	Needle	Block
Crystal size (mm)	0.48 × 0.24 × 0.18	0.46 × 0.28 × 0.22	0.56 × 0.08 × 0.04	0.55 × 0.10 × 0.06	0.17 × 0.10 × 0.05
Data collection					
Absorption correction	Multi-scan (Empirical SCALE3 ABSPACK)	Multi-scan (Empirical SCALE3 ABSPACK)	Multi-scan (Empirical SCALE3 ABSPACK)	Analytical (ABSFAC, Clark & Reid, 1998)	Analytical (ABSFAC, Clark & Reid, 1998)
T_{min}, T_{max}	0.859, 1.000	0.922, 1.000	0.85, 1.00	0.919, 0.983	0.947, 0.984
Measured, independent, observed [$I > 2\sigma(I)$] reflections	7681, 2325, 1594	21867, 11150, 7857	16862, 2412, 1308	15313, 8956, 4067	8847, 2480, 917
R_{int}	0.027	0.015	0.066	0.035	0.097
$(\sin\theta/\lambda)_{max}$ (Å^{-1})	0.648	0.693	0.647	0.640	0.651
Refinement					
$R[F^2>2\sigma(F^2)]$, $wR(F^2)$, *S*	0.038, 0.098, 1.03	0.039, 0.113, 1.07	0.041, 0.089, 0.86	0.043, 0.084, 0.76	0.050, 0.097, 0.76
No. of reflections	2325	11150	2412	8956	2480
No. of parameters	150	593	149	594	166
No. of restraints	0	0	0	0	3
$\Delta\rangle_{max}$, $\Delta\rangle_{min}$ (e.Å^{-3})	0.36, -0.40	0.41, -0.56	0.18, -0.15	0.16, -0.20	0.29, -0.19

Clxx isomers	Clom	Clpo_O (polymorph)	Clpo_N (polymorph)	Clmo	Cloo
Crystal data					
Chemical formula	$C_{12}H_9ClN_2O$	$C_{12}H_9ClN_2O$	$C_{12}H_9ClN_2O$	$C_{12}H_9ClN_2O$	$C_{12}H_9ClN_2O$
M_r	232.66	232.66	232.66	232.66	232.66
Crystal system, space group	Monoclinic, *C*2/*c*	Monoclinic, *C*2/*c*	Monoclinic, *C*2/*c*	Triclinic, $P\bar{1}$	Monoclinic, *C*2/*c*
a, *b*, *c* (Å)	18.1011(4), 10.8717(2), 11.4678(3)	26.611(2), 5.2075(4), 15.4341(13)	27.0371(3), 8.2490(1), 10.7506(1)	5.8841(3), 7.3302(5), 12.6907(8)	21.8178(9), 6.6955(3), 14.8776(6)
α, β, γ (°)	90, 91.302(2), 90	90, 93.485(7), 90	90, 112.0204 (14), 90	77.717(6), 82.504(5), 88.442(5)	90, 94.541(4), 90
V (Å^3)	2256.16(9)	2134.8(3)	2222.78(5)	530.27(6)	2166.51(16)
Z	8	8	8	2	8
Radiation type	Mo *K*α	Mo *K*α	Cu *K*α	Mo *K*α	Mo *K*α
μ (mm^{-1})	0.32	0.34	2.87	0.34	0.33
Crystal shape	Block	Block	Block	Block	Block
Crystal size (mm)	0.22 × 0.20 × 0.15	0.35 × 0.23 × 0.14	0.36 × 0.18 × 0.11	0.37 × 0.29 × 0.11	0.52 × 0.35 × 0.29
Data collection					
Absorption correction	Analytical (ABSFAC, Clark & Reid, 1998)	Multi-scan (Empirical SCALE3 ABSPACK)	Analytical (ABSFAC, Clark & Reid, 1998)	Multi-scan (Empirical SCALE3 ABSPACK)	Analytical (ABSFAC, Clark & Reid, 1998)
T_{min}, T_{max}	0.957, 0.976	0.98, 1.00	0.481, 0.747	0.90, 1.00	0.877, 0.920
Measured, independent and observed [$I > 2\sigma(I)$] reflections	8589, 2476, 1702	7164, 2280, 1841	5698, 1751, 1658	4063, 2303, 1890	9415, 2816, 2212
R_{int}	0.025	0.018	0.013	0.014	0.015
$(\sin\theta/\lambda)_{max}$ (Å^{-1})	0.650	0.642	0.575	0.655	0.686
Refinement					
$R[F^2 > 2\sigma(F^2)]$, $wR(F^2)$, *S*	0.034, 0.089, 1.00	0.031, 0.089, 1.08	0.032, 0.093, 1.06	0.034, 0.100, 1.09	0.036, 0.110, 1.09
No. of reflections	2476	2280	1751	2303	2816
No. of parameters	149	150	150	150	149
No. of restraints	0	0	0	0	0
$\Delta\rangle_{max}$, $\Delta\rangle_{min}$ (e.Å^{-3})	0.22, -0.28	0.17, -0.18	0.16, -0.25	0.18, -0.20	0.25, -0.26

Computer programs: *CrysAlis PRO*, Oxford Diffraction Ltd., Version 1.171.33.55 (release 05-01-2010 CrysAlis171 .NET), Version 1.171.34.40 (release 27-08-2010 CrysAlis171 .NET), *SHELXS14*/7 (Sheldrick, 2014), *SHELXL14*/7 (Sheldrick, 2014), *PLATON* (Spek, 2009), *SHELXL14*/7.

TABLE S2A: SELECTED HYDROGEN-BOND PARAMETERS (Å,°)

D—H···*A*	*D*—H (Å)	H···*A* (Å)	*D*···*A* (Å)	*D*—H···*A* (°)
Clpp				
N1—H1···N24^{i}	0.827 (19)	2.441 (19)	3.114 (2)	139.2 (17)
C26—H26···O1	0.93	2.35	2.891 (2)	117
Clmp				
N1A—H1A···N24D	0.836 (15)	2.132 (15)	2.9431 (16)	163.4 (14)
N1B—H1B···N24C	0.848 (15)	2.210 (16)	3.0120 (16)	157.7 (14)
N1C—H1C···N24B^{ii}	0.853 (15)	2.316 (15)	3.1576 (16)	169.1 (13)
N1D—H1D···N24A^{iii}	0.812 (15)	2.388 (15)	3.1913 (16)	170.4 (14)
C22A—H22A···O1A	0.93	2.35	2.8709 (16)	115
C22B—H22B···O1B	0.93	2.35	2.8698 (17)	115
C22C—H22C···O1C	0.93	2.22	2.8073 (17)	120
C22D—H22D···O1D	0.93	2.23	2.8155 (18)	121
C12C—H12C···N24B^{ii}	0.93	2.37	3.2961 (18)	173
C12D—H12D···N24A^{iii}	0.93	2.38	3.2761 (18)	161
C14B—H14B···O1C^{iv}	0.93	2.59	3.2416 (17)	127
C16A—H16A···O1A^{v}	0.93	2.47	3.3516 (17)	160
Clop				
N1—H1···N24^{vi}	0.846 (19)	2.17 (2)	3.010 (3)	175.9 (18)
C15—H15···O1^{vii}	0.93	2.50	3.266 (3)	139
C26—H26···O1	0.93	2.28	2.860 (3)	120
Clpm				
N1A—H1A···N23B	0.97 (4)	2.24 (4)	3.184 (4)	165 (3)
N1B—H1B···N23C	0.80 (4)	2.43 (4)	3.203 (4)	164 (4)
N1C—H1C···N23D	0.74 (3)	2.43 (3)	3.151 (4)	166 (3)
N1D—H1D···N23A^{viii}	0.79 (3)	2.37 (4)	3.150 (4)	168 (3)
C16A-H16A···N23B	0.93	2.48	3.386(4)	164
C16B-H16B···N23C	0.93	2.46	3.356(4)	162
Clmm_H_2O				
N1—H1···O1W^{ix}	0.817 (18)	2.11 (2)	2.892 (4)	161 (3)
O1W—H1W···N23	0.905 (18)	1.96 (2)	2.858 (4)	169 (3)
O1W—H2W···O1^{i}	0.876 (19)	2.07 (3)	2.890 (4)	156 (5)
C26—H26···O1	0.93	2.38	2.871 (4)	113
Clom				
N1—H1···N23^{x}	0.835 (16)	2.073 (17)	2.9058 (17)	175.3 (15)

C22—H22···O1	0.93	2.31	2.8844 (18)	120
Clpo_O polymorph				
N1—H1···O1^{xi}	0.807 (17)	2.368 (17)	3.1296 (14)	157.7 (15)
C15—H15···N22^{xii}	0.93	2.60	3.5199 (18)	168
C26—H26···O1	0.93	2.37	2.8954 (17)	116
Clpo_N polymorph				
N1—H1···N22^{xiii}	0.762 (18)	2.337 (18)	3.0715 (19)	162.4 (17)
C15—H15···O1^{xiv}	0.93	2.66	3.329 (2)	129
C26—H26···O1	0.93	2.24	2.840 (2)	121
Clmo				
N1—H1···N22^{xv}	0.84(2)	2.45(2)	3.1990 (17)	148.9(17)
C26—H26···O1	0.93	2.31	2.8906 (17)	120
Cloo				
N1—H1···N22^{xvi}	0.835 (16)	2.219 (16)	3.0485 (14)	171.9 (14)
C26—H26···O1	0.93	2.28	2.8700 (16)	121
C16-H16···Cg1^{xvii}	0.93	2.73	3.5414(15)	146
C23-H23···Cg1^{xvi}	0.93	2.70	3.4233(15)	135

Cg1 is the ring centroid of the benzene ring {C11,...,C16}.

Symmetry code(s): (*i*) -*x*+1, *y*+1/2, -*z*+1/2; (*ii*) *x*-1, *y*, *z*; (*iii*) *x*+1, *y*, *z*; (*iv*) *x*, *y*-1, *z*; (*v*) -*x*, -*y*+3, -*z*+1; (*vi*) -*x*+1/2, *y*+1/2, *z*; (*vii*) -*x*-1/2, *y*+1/2, *z*; (*viii*) *x*-1, *y*+1, *z*; (*ix*) *x*, -*y*+1/2, *z*-1/2; (*x*) *x*, -*y*+1, *z*-1/2; (*xi*) *x*, *y*+1, *z*; (*xii*) -*x*+1/2, -*y*+3/2, -*z*; (*xiii*) -*x*, *y*, -*z*-1/2; (*xiv*) *x*, -*y*, *z*+1/2; (*xv*) -*x*+2, -*y*+1, -*z*; (*xvi*) -*x*, *y*, -*z*+1/2; (*xvii*) 1/2-x, 1/2+y, 1/2-z *and additional interactions in* ***Table 2b*** (*xviii*) 2-x, -y, 1-z; (*xix*) x, 1/2-y, 1/2+z; (*xx*) 1-x, 2-y, -z; (*xxi*) 1/2+x, y, 1/2-z; (*xxii*) 1-x, 1-y, 1-z; (*xxiii*) -x, -y, -1-z; (*xxiv*) -x, -y, 2-z; (*xxv*) = 1/2-x, 1/2-y, -z; (*xxvii*) 1-x, 1-y, -z; (*xxvii*) -x, 2-y, -z.

In the manuscript the symmetry codes quoted correspond to those in the **Table 2a** (above) although given the crystal structure discussion and its discussion then they may not actually be in order in the text.

TABLE S2B: INTERACTIONS AND CONTACTS(Å,°)[25-30,40-42] (PLUS HALOGEN BONDING)[31-39]:

Clxx	***Interaction type***	***D*—H or D—X**	**H···*A***	***D*···*A* or *X*···*A***	***D*—H···*A* or *C*—X···*A***
Clpp*	C26—H26···Cg1[xviii]	0.93	2.84	3.5145(19)	130
	C14—Cl14···C21[xix]	1.7351(18) for C—Cl	/	3.3269(18)	150.10(7)°
Clmp	C1C···C12C[xx]	Ring stacking type	/	3.360(2) for C···C	/
	C14C···C21C[xx]	Ring stacking type	/	3.323(2) for C···C	/
Clop	C12—Cl12···O1=C1[xxi]	Cl···O halogen bond	/	3.1104(18)	161.08(8)/111.27(13)
Clpm	C15A—H15A···Cl4A[xxii]	C—H···Cl contact	2.94	3.807(4)	156
Clmm•H_2O	C15—H15···C15[xxiii]	(C15—H15···C15)[xxiii]	2.85	3.402(5)	119 (C15—H15···C15)[xxiii]
Clom	Cl12···O1	Intramolecular	/	3.1811(13)	/
	C—Cl···Cl—C[xxiv]	Repulsive - type I Cl...Cl	/	3.3699(10)	167.66(6)
Clpo_O	C16...C1=O1[xxv]	π···(C=O)[xxv] type	/	3.3488(19)	/
Clpo_N	C15—H15···C12[xiv]	C—H···C type	2.85	3.691(2)	151
Clmo	C12—H12···C24[xxvi]	C—H···C type	2.84	3.504(2)	130
Cloo	C24...C26[xxvii]	π···π stacking type	/	3.3049(18)	/

* = The C14-Cl14...π(pyridine) contact has angle dimensions of C14-Cl14...π(centroid) = 163.34(7)° in **Clpp**.

The value quoted in **Table S2b** refers to the closest Cl···C contact as C14—Cl14···C21[xix]

TABLE S2C: SELECTED INTERMOLECULAR INTERACTIONS FOR THE MAIN PAPER.

Clxx	*D*—H···*A*	*D*—H (Å)	H···*A* (Å)	*D*···*A* (Å)	*D*—H···*A* (°)
Clpp	N1—H1···N24^{i}	0.827 (19)	2.441 (19)	3.114 (2)	139.2 (17)
Clmp	N1A—H1A···N24D	0.836 (15)	2.132 (15)	2.9431 (16)	163.4 (14)
	N1B—H1B···N24C	0.848 (15)	2.210 (16)	3.0120 (16)	157.7 (14)
	N1C—H1C···N24B^{ii}	0.853 (15)	2.316 (15)	3.1576 (16)	169.1 (13)
	N1D—H1D···N24A^{iii}	0.812 (15)	2.388 (15)	3.1913 (16)	170.4 (14)
	C12C—H12C···N24B^{ii}	0.93	2.37	3.2961 (18)	173
	C12D—H12D···N24A^{iii}	0.93	2.38	3.2761 (18)	161
Clop	N1—H1···N24^{vi}	0.846 (19)	2.17 (2)	3.010 (3)	175.9 (18)
	C15—H15···O1^{vii}	0.93	2.50	3.266 (3)	139
Clpm	N1A—H1A···N23B	0.97 (4)	2.24 (4)	3.184 (4)	165 (3)
	N1B—H1B···N23C	0.80 (4)	2.43 (4)	3.203 (4)	164 (4)
	N1C—H1C···N23D	0.74 (3)	2.43 (3)	3.151 (4)	166 (3)
	N1D—H1D···N23A^{viii}	0.79 (3)	2.37 (4)	3.150 (4)	168 (3)
Clmm	N1—H1···O1W^{ix}	0.817 (18)	2.11 (2)	2.892 (4)	161 (3)
	O1W—H1W···N23	0.905 (18)	1.96 (2)	2.858 (4)	169 (3)
	O1W—H2W···O1^{i}	0.876 (19)	2.07 (3)	2.890 (4)	156 (5)
Clom	N1—H1···N23^{x}	0.835 (16)	2.073 (17)	2.9058 (17)	175.3 (15)
Clpo_O	N1—H1···O1^{xi}	0.807 (17)	2.368 (17)	3.1296 (14)	157.7 (15)
Clpo_N	N1—H1···N22^{xiii}	0.762 (18)	2.337 (18)	3.0715 (19)	162.4 (17)
Clmo	N1—H1···N22^{xv}	0.84 (2)	2.45 (2)	3.1990 (17)	148.9 (17)
Cloo	N1—H1···N22^{xvi}	0.835 (16)	2.219 (16)	3.0485 (14)	171.9 (14)

In the manuscript the symmetry codes quoted correspond to those for the most important intermolecular interactions in the Table (above) although given the crystal structure discussion and its development they may not actually seem in order.

FIGURE S3. : ENLARGED FORMAT FOR EASE OF VIEWING/COMPARISONS

The Potential Energy Surface conformational analysis for **Clxx** molecules optimized in the *gas phase*: the equivalent solid-state angle is shown by (•) with, if applicable, an assigned identifier.

Clpp

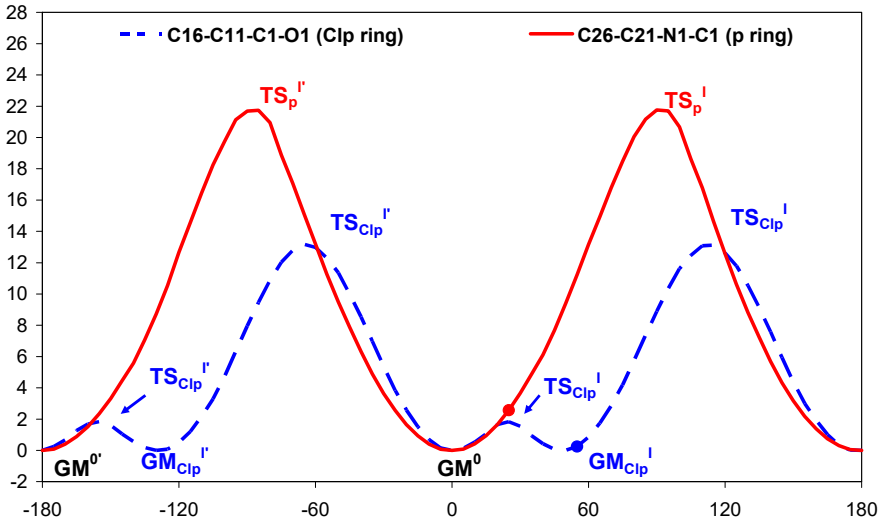

Clmp

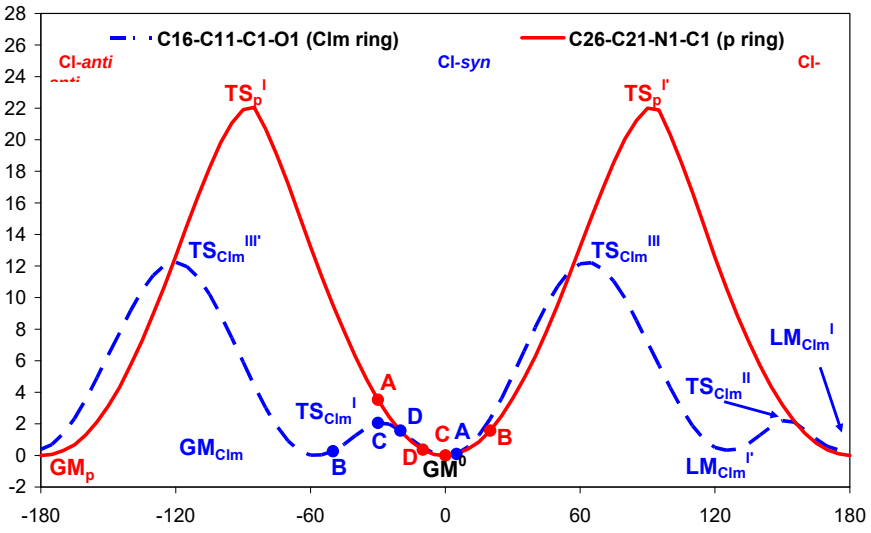

Clop

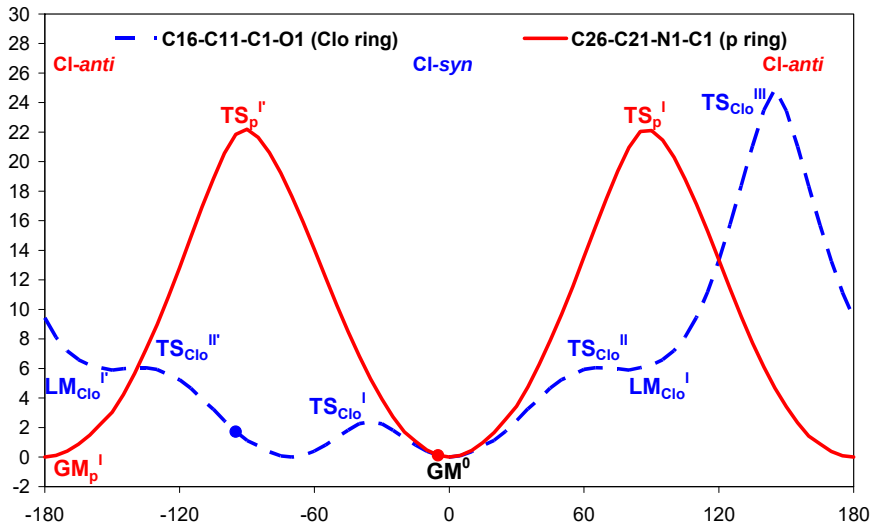

Clpm

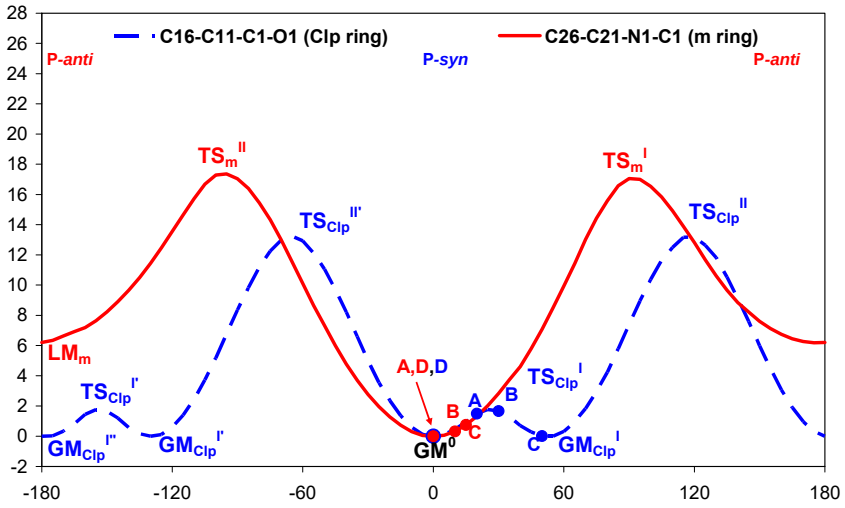

Clmm

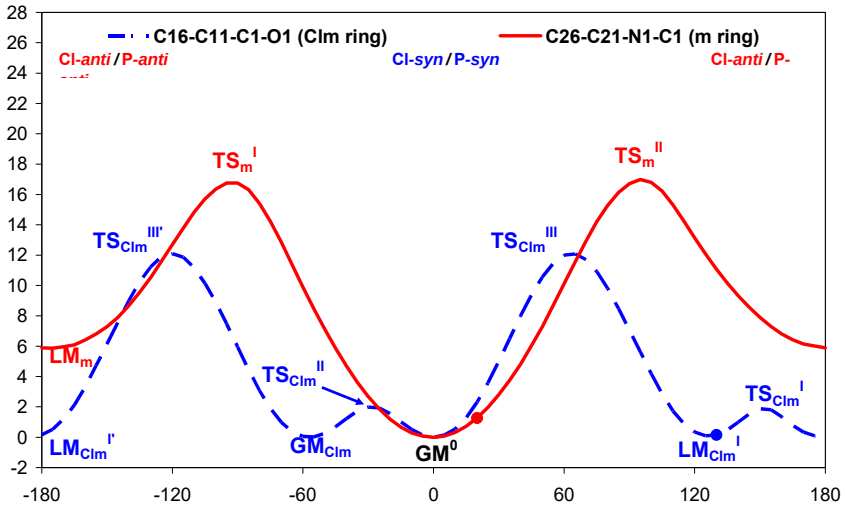

Clom

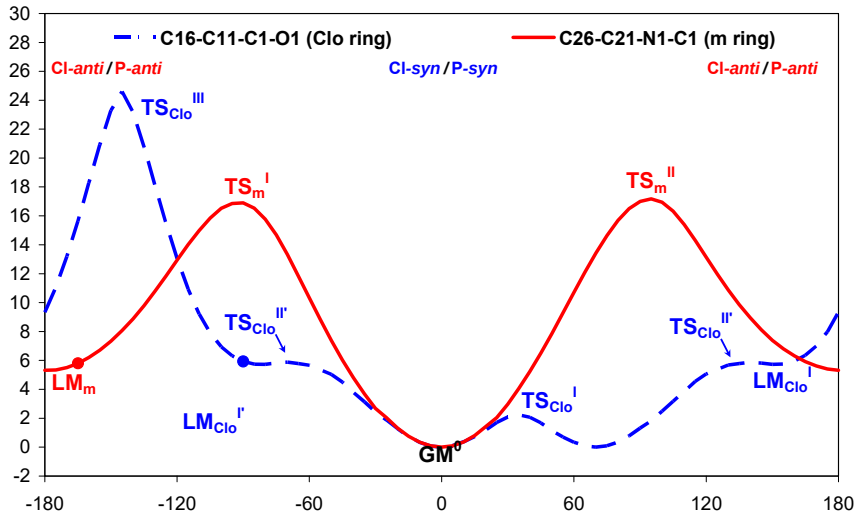
C16-C11-C1-O1 (Clo ring)
C26-C21-N1-C1 (m ring)
Cl-anti / P-anti
Cl-syn / P-syn
Cl-anti / P-anti
TS_Clo III
TS_m I
TS_m II
TS_Clo II'
TS_Clo II'
LM_m
LM_Clo I'
TS_Clo I
LM_Clo I
GM0

Clpo

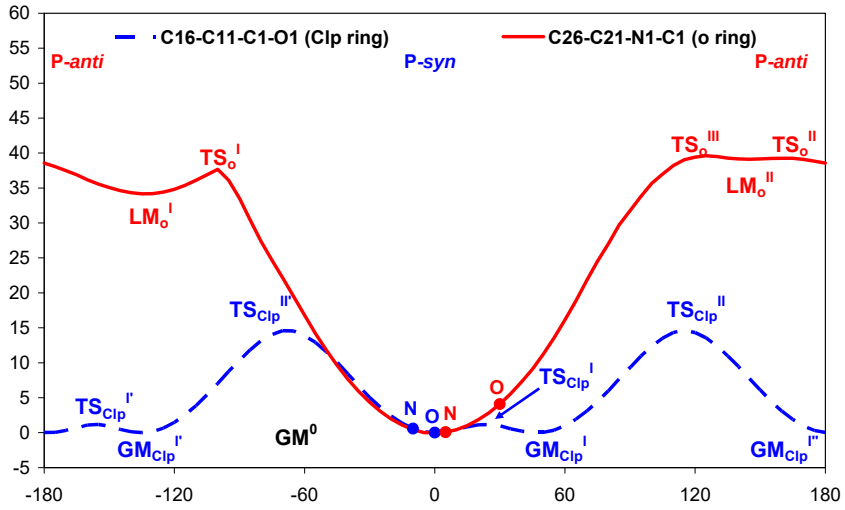
C16-C11-C1-O1 (Clp ring)
C26-C21-N1-C1 (o ring)
P-anti
P-syn
P-anti
TS_o I
TS_o III
TS_o II
LM_o II
LM_o I
TS_Clp II'
TS_Clp II
TS_Clp I
O
TS_Clp I'
N
O
N
GM_Clp I'
GM0
GM_Clp I
GM_Clp I''

Clmo

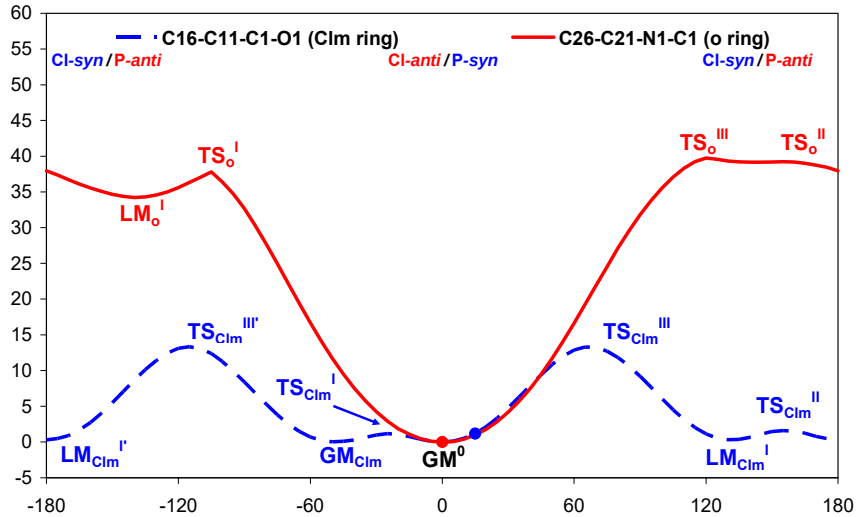
C16-C11-C1-O1 (Clm ring)
C26-C21-N1-C1 (o ring)
Cl-syn / P-anti
Cl-anti / P-syn
Cl-syn / P-anti
TS_o I
TS_o III
TS_o II
LM_o I
TS_Clm III'
TS_Clm III
TS_Clm I
TS_Clm II
LM_Clm I'
GM_Clm
GM0
LM_Clm I

Cloo

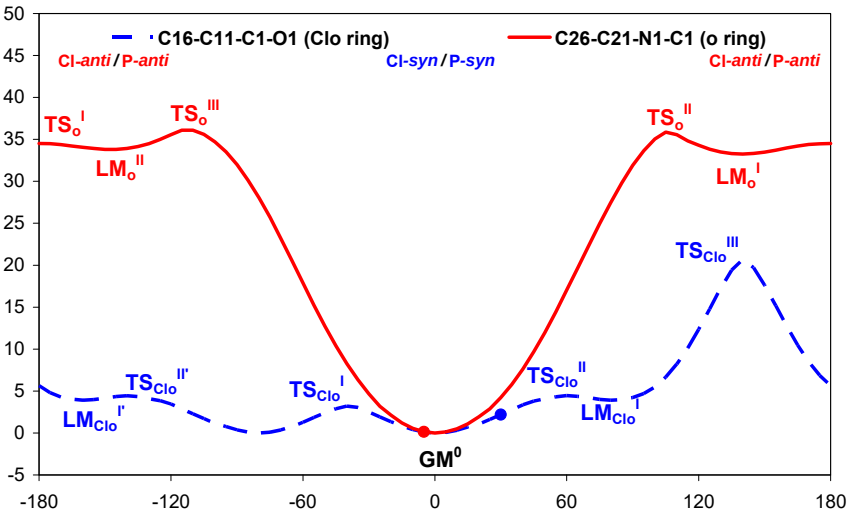
C16-C11-C1-O1 (Clo ring)
C26-C21-N1-C1 (o ring)
Cl-anti / P-anti
Cl-syn / P-syn
Cl-anti / P-anti
TS$_o^I$
TS$_o^{III}$
LM$_o^{II}$
TS$_o^{II}$
LM$_o^I$
TS$_{Clo}^{III}$
TS$_{Clo}^{II'}$
TS$_{Clo}^I$
TS$_{Clo}^{II}$
LM$_{Clo}^{I'}$
LM$_{Clo}^I$
GM^0
50
45
40
35
30
25
20
15
10
5
0
-5
-180
-120
-60
0
60
120
180

TABLE S3 SUPPLEMENTARY MELTING POINT

Melting points: Comparisons of the **Mxx**, **NxxM**, **Fxx** and **NxxF** [3 × 3] isomer grids.

		benzamides			pyridinecarboxamides			
	Mxx	Mp	Mm	Mo	No	Nm	Np	NxxM
M	p	181♦	106	129	105	148	162♦	pM
M	m	128	91	108	50*	115	142	mM
M	o	105	79*	116	65	107	125	oM
F	o	120	77*	85	107	117	140♦	oF
F	m	150, 148	151	89	78*	122	132	mF
F	p	187♦	186	135	94	133	135	pF
	Fxx[b]	Fp	Fm	Fo	No	Nm	Np	NxxF

Average melting point range for all 37 compounds with highest denoted by ♦ and lowest by *
- Green labels highlight the **N-H...N** interaction
- Orange labels the **N-H...O=C** hydrogen bonds
- Melting points for compounds in non-centrosymmetric space groups are underlined.

Graph of melting point trends in series of benzamides (**Fxx**, **Mxx**) and their amide-reversed bridged pyridinecarboxamides (**NxxF**, **NxxM**) for comparisons with **Clxx** (below).

Melting point averages and ranges for Clxx

Clxx isomers	Clp	Clm	Clo
para	207♦	187	169
meta	151	113#	136
ortho	133	100*	136

as taken from the following

Clxx (mp range)	Clp	Clm	Clo
para	206.2-208.4	185.4-187.2	167.9-169.9
meta	150.1-151.3	112.4-113.9	134.5-137.8
ortho	131.5-134.5	95-105	134.4-138.0

From Chloe Violin results and comparisons:

Melting point averages for Brxx

Brxx isomers	Brp	Brm	Bro
para	188♦	162	177
meta	159	122#	119
ortho	132	118*	**30**

Figure S4
Scatterplot of the melting point temperature and computed lattice electrostatic energy.

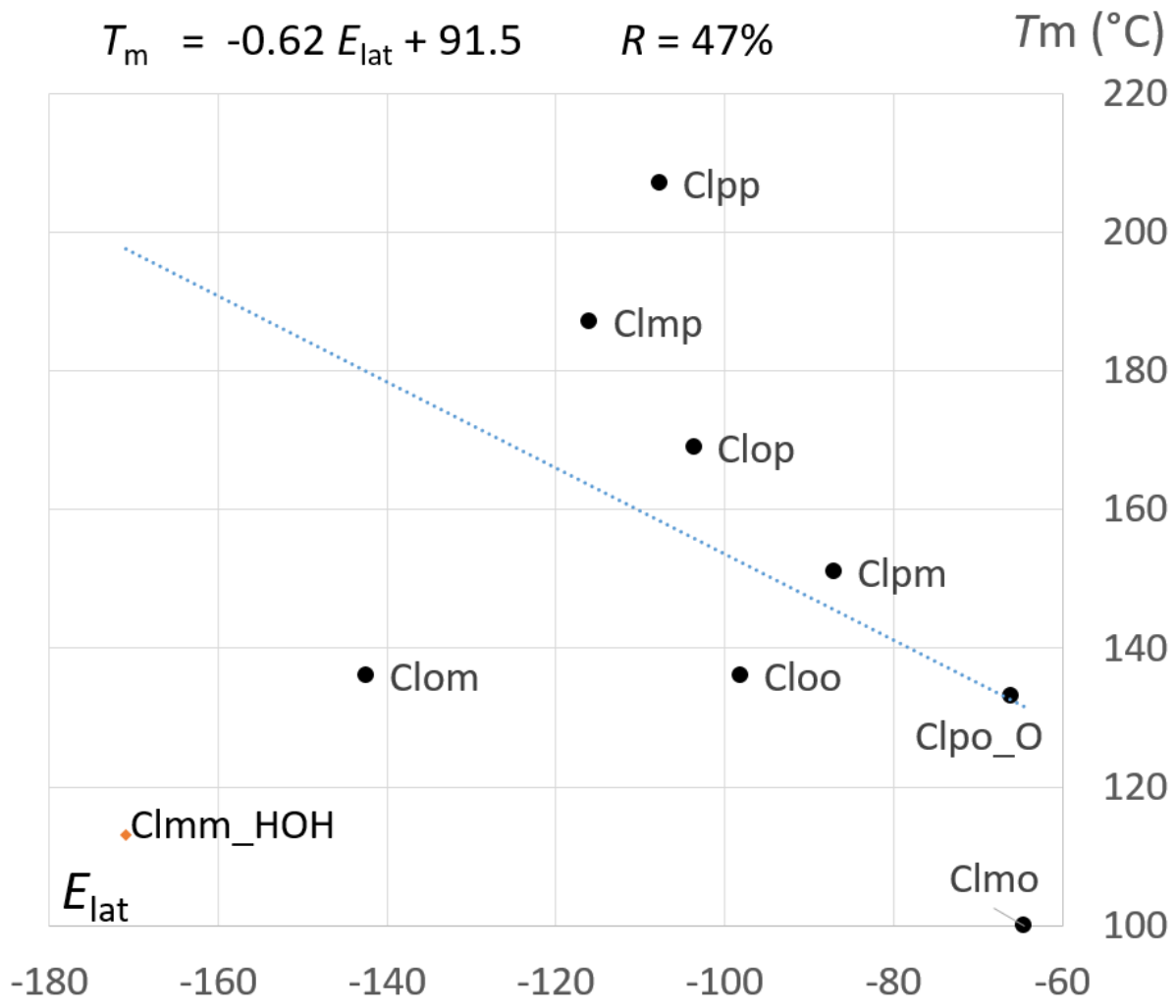

Figure S5

Scatterplot of the experimental T_m and fitted T_{fit} fusion temperatures. The double linear regression was performed on the *ortho*-/*meta*-/*para*-positions descriptor f(Clxy) and E_{lat}.

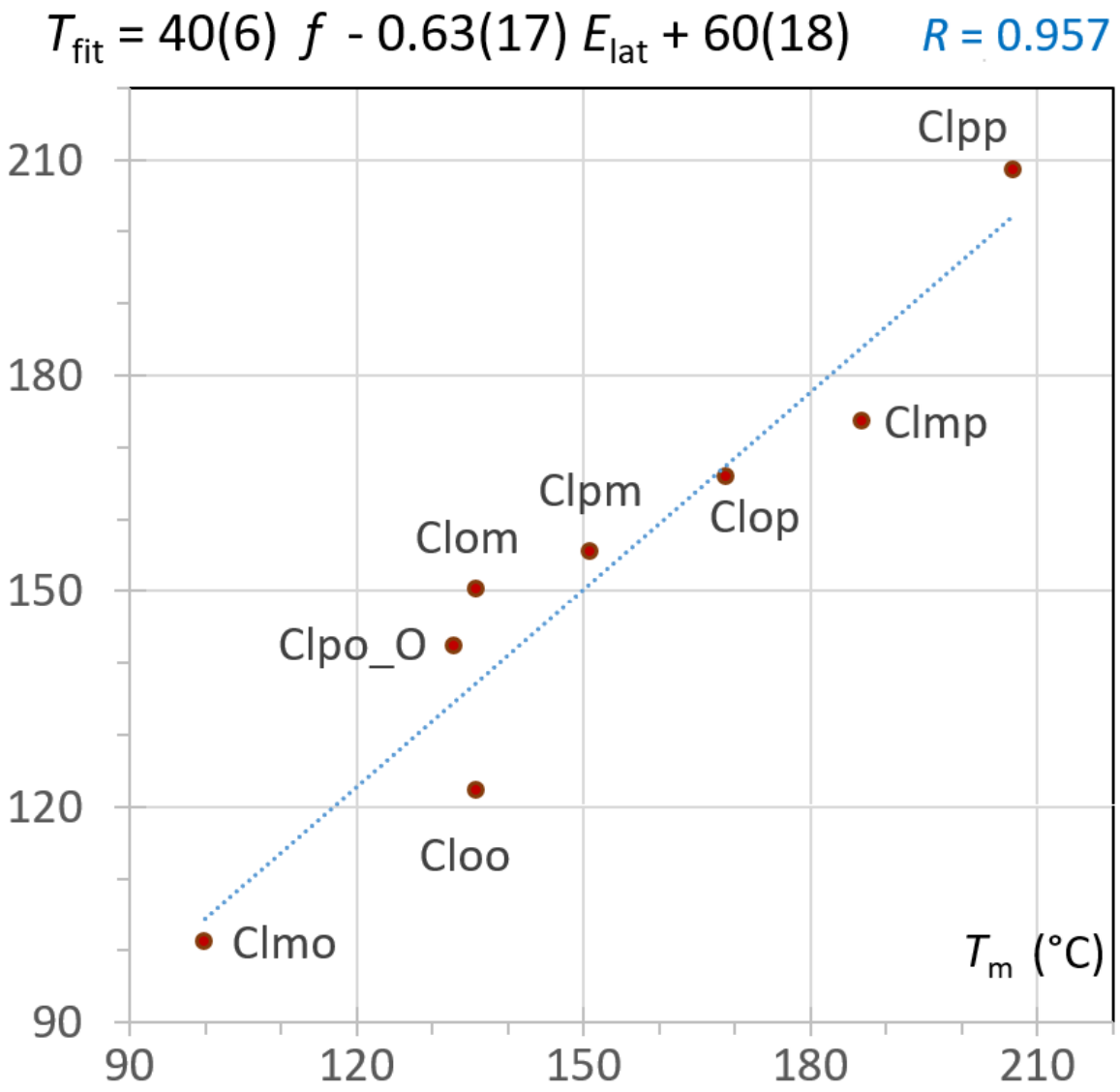

Figure S6.
Scatterplot of lattice E_{lat} and density

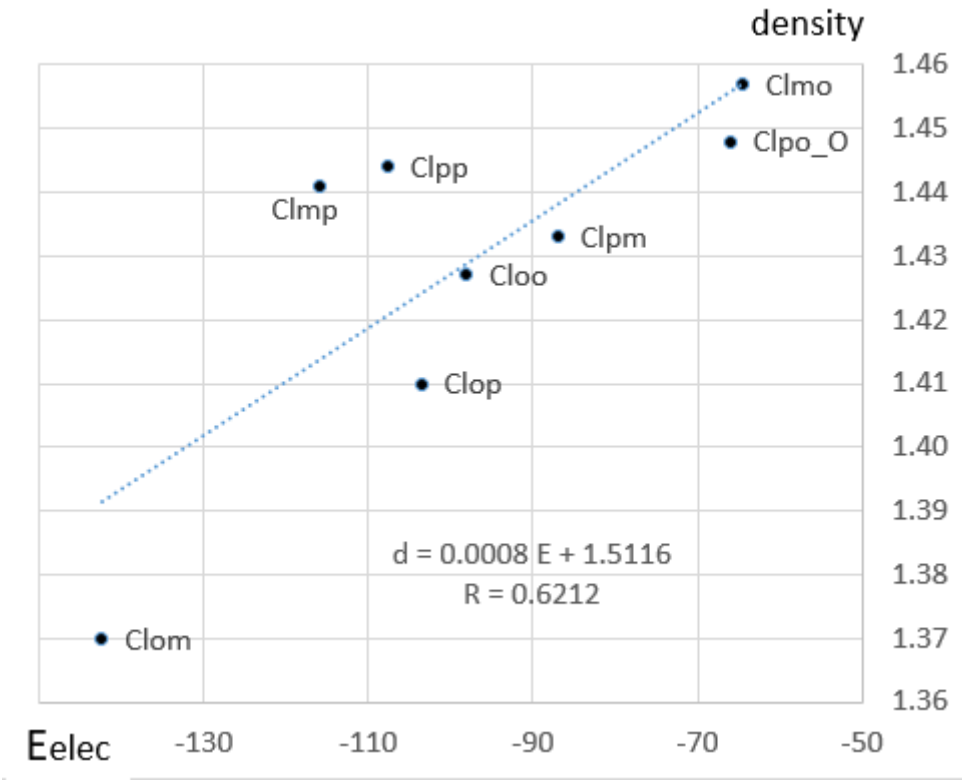

Figure S7

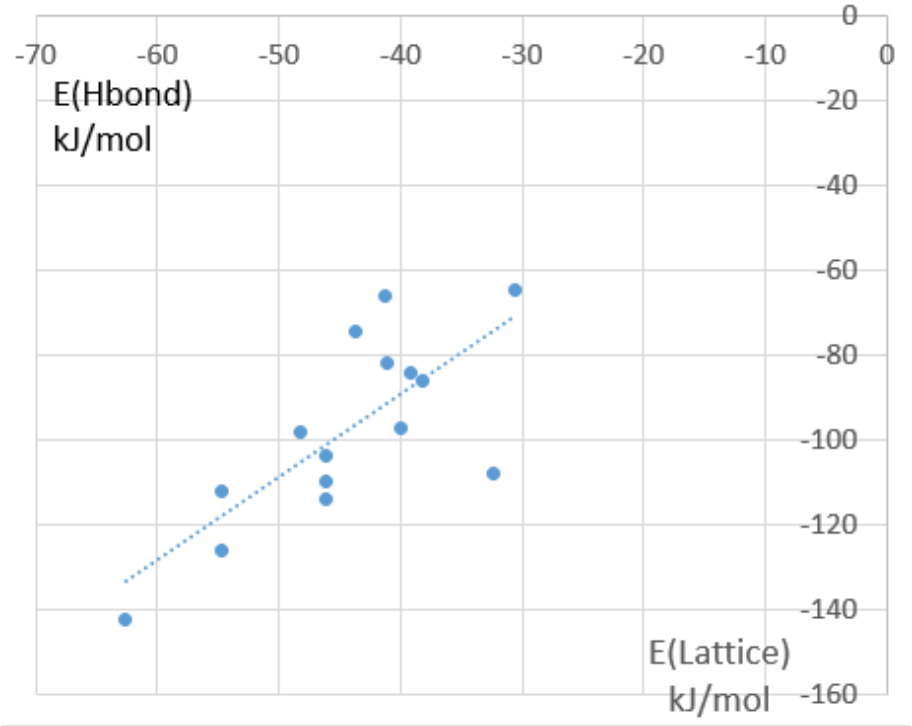

Figure S8

Contribution of the N-H…N and N-H…O strong hydrogen bonds to the lattice electrostatic energy.

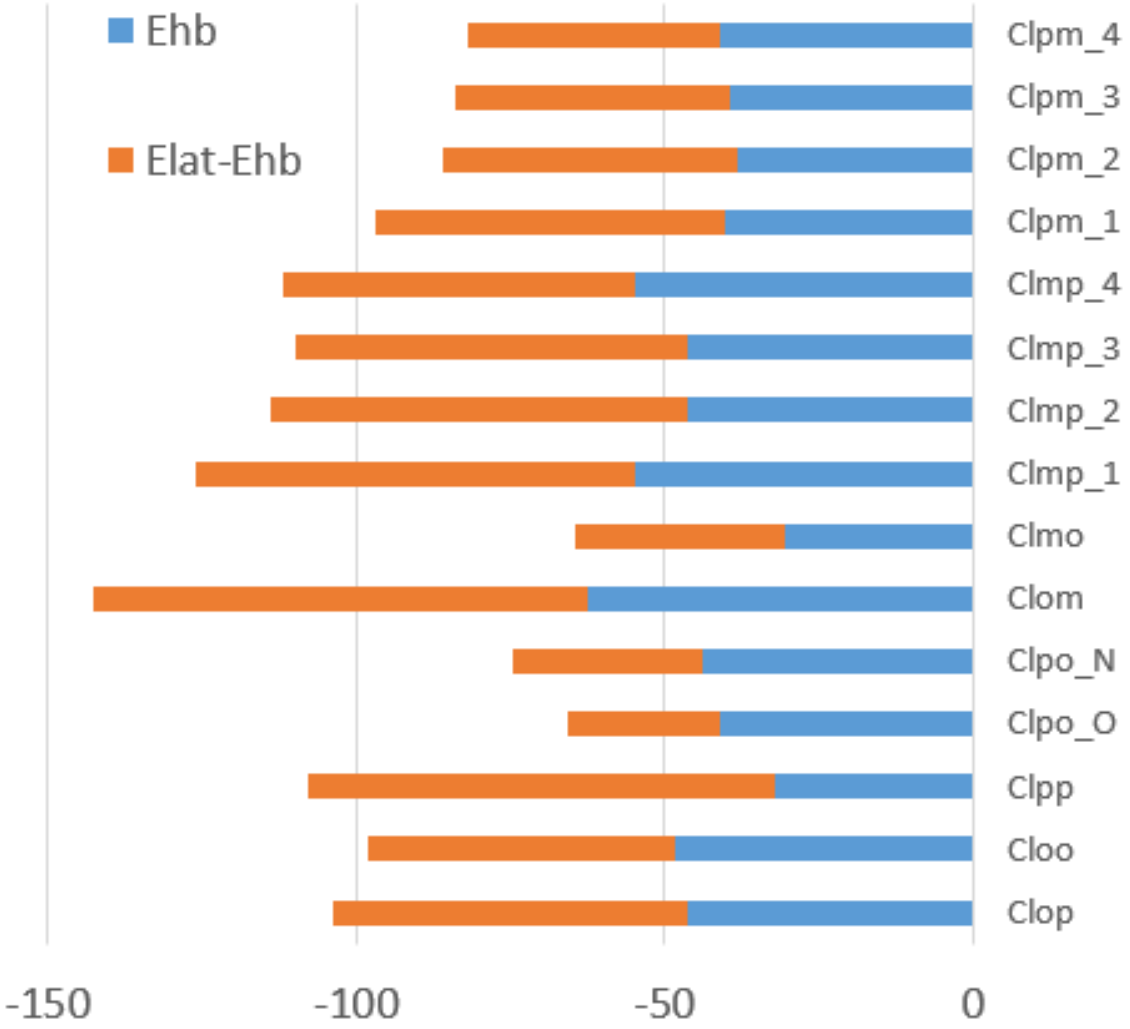

Table S9. Proportion of contact types (%) in the 10 **Clxx** crystal structures.

atom	C	H_C	Cl	N	O	H_N
C	12.1					
H_C	32.6	6.5				**Clmo**
Cl	4.8	23.6	0.1			
N	1.9	3.5	0.0	0.0		
O	4.6	3.3	0.0	0.9	0.0	
H_N	0.2	0.2	0.0	3.8	1.4	0.6
C	11.7					
H_C	32.2	11.9				**Clom**
Cl	5.0	13.0	3.6			
N	3.8	2.6	0.0	0.0		
O	1.9	8.0	0.0	0.0	0.0	
H_N	1.3	0.7	0.0	4.5	0.0	0.0
C	15.3					
H_C	26.3	13.6				**Cloo**
Cl	4.4	17.7	0.2			
N	0.8	1.5	2.8	0.0		
O	4.7	6.3	0.0	0.0	0.0	
H_N	0.1	0.1	1.1	4.6	0.0	0.7
C	15.9					
H_C	19.9	18.7				**Clop**
Cl	10.1	11.7	0.0			
N	2.4	3.9	0.0	0.0		
O	1.7	5.9	3.3	0.0	0.0	
H_N	1.4	1.0	0.0	4.1	0.0	0.0
C	18.2					
H_C	20.9	13.3				**Clpo_N**
Cl	7.3	17.3	1.4			
N	2.7	2.9	0.0	0.1		
O	1.8	8.1	0.1	0.0	0.0	
H_N	0.4	0.7	0.0	4.3	0.0	0.7
C	11.6					
H_C	30.9	8.1				**Clpo_O**
Cl	7.7	17.8	1.0			
N	3.8	7.2	0.0	0.0		
O	3.4	1.9	0.0	0.2	0.0	
H_N	0.7	1.3	0.0	0.0	4.5	0.0
C	8.2					
H_C	37.2	7.1				**Clpp**
Cl	12.6	13.9	0.0			
N	1.1	4.5	0.9	0.3		
O	3.2	5.0	0.0	0.1	0.0	
H_N	0.0	0.3	0.0	3.8	2.0	0.0

C_{xy}	C	H_C	Cl	N	O	H_N
C	18.2					
H_C	17.4	13.5			**Clmp**	
Cl	9.5	16.2	2.2			
N	3.8	2.8	0.2	0.1		
O	1.7	8.2	0.3	0.1	0.0	
H_N	1.3	0.3	0.0	4.2	0.1	0.0
C	20.2					
H_C	16.6	12.6			**Clpm**	
Cl	7.8	17.3	2.1			
N	4.0	4.3	0.0	0.0		
O	1.7	6.8	0.4	0.0	0.4	
H_N	1.4	1.1	0.0	3.3	0.0	0.0

and

C_{xy}	C	H_C	Cl	N	O	$H_{N/O}$
C	18.6					
H_C	12.5	9.9			**Clmm_HOH**	
Cl	3.8	14.0	0.3			
N	3.3	1.0	1.3	0.0		
O	1.2	8.9	2.6	0.0	0.0	
$H_{N/O}$	2.6	6.8	1.8	4.5	6.6	0.3

Table S10. Contact enrichment ratios in the **Clxx** crystals.

Exy	C	H_C	Cl	N	O	H_N
C	1.0					
H_C	1.3	0.5			**Clmo**	
Cl	0.5	2.2	0			
N	0.6	0.9	0	0		
O	1.3	0.9	0	1.7	0	
H_N	0.1	0.1	0	11.2	4	5.2
C	1.0					
H_C	1.2	0.7			**Clom**	
Cl	0.6	1.3	2.3			
N	1	0.6	0	0		
O	0.6	2	0	0	0	
H_N	0.6	0.3	0	12.8	0	0
C	1.4					
H_C	1.0	0.9			**Cloo**	
Cl	0.5	1.7	0.1			
N	0.2	0.4	2.2	0		
O	1.3	1.4	0	0	0	
H_N	0	0.1	1.2	13.1	0	5.2
C	1.4					
H_C	0.7	1.2			**Clop**	
Cl	1.2	1.2	0			
N	0.7	0.9	0	0		
O	0.5	1.4	2.4	0	0	
H_N	0.6	0.4	0	12.2	0	0
C	1.5					
H_C	0.8	0.9			**Clpo_N**	
Cl	0.8	1.7	0.7			
N	0.8	0.8	0	0.4		
O	0.5	2.1	0.1	0	0	
H_N	0.2	0.3	0	12.8	0	6
C	1.0					
H_C	1.2	0.6			**Clpo_O**	
Cl	0.8	1.7	0.6			
N	1.0	1.7	0	0		
O	1.0	0.5	0	0.4	0	
H_N	0.3	0.5	0	0	13.9	0

C	0.7					
H_C	1.4	0.5		**Clpp**		
Cl	1.3	1.4	0			
N	0.3	1.1	0.6	1.1		
O	0.9	1.3	0	0.2	0	
H_N	0	0.1	0	11.4	6.4	0
C	1.5					
H_C	0.7	1.1		**Clmp**		
Cl	0.9	1.5	0.9			
N	1	0.7	0.1	0.3		
O	0.5	2.2	0.2	0.2	0	
H_N	0.6	0.1	0	12.7	0.4	0
C	1.6					
H_C	0.7	1		**Clpm**		
Cl	0.7	1.6	1			
N	1	1	0	0		
O	0.5	2	0.3	0	1.7	
H_N	0.7	0.5	0	9.6	0	0.3

and

Exy	**C**	**H_C**	**Cl**	**N**	**O**	**$H_{N/O}$**
C	2.0					
Hc	0.7	1.0		**Clmm•H_2O**		
Cl	0.5	1.8	0.2			
N	1.1	0.3	1.1	0.0		
O	0.2	1.5	1.1	0.0	0.0	
$H_{N/O}$	0.4	0.9	0.7	3.9	3.0	0.2

Table S11

The % contacts are regrouped by interactions between hydrophobic (C, H_C, Cl) and hydrophilic (O, N, H_N) atom types as well as cross interactions.

% contacts	hydrophobic	hydrophilic	cross
Clmo	80	7	13
Clom	77	5	18
Cloo	77.5	5	17.5
Clop	76	4	20
Clpo_N	78	5	17
Clpo_O	77	5	18
Clpp	79	6	14
Clmp	77	4.5	18.5
Clpm	76.5	4	19.5
average	78	5	17
ssd	1.4	1.2	2.1

Table S12.

Correlation coefficient *c* between the different enrichment ratios of the nine non-hydrated **Clxx** crystal structures. The *c* values with the largest magnitude are in bold characters. Numbers highlighted in yellow are discussed in the manuscript.

Contact	C:H_N	C:C	N:H_N	N:C	N:N	O:H_N	O:C	O:N	O:O	Cl:H_N
H_N:H_N	-0.65	0.23	0.31	-0.45	-0.14	-0.24	0.51	0.35	-0.23	0.46
C:H_N		-0.65	0.23	0.31	-0.45	-0.14	-0.24	0.51	0.35	-0.23
C:C			0.49	0.01	**0.79**	-0.39	-0.34	**-0.79**	-0.40	0.44
N:H_N				0.32	0.31	-0.45	-0.66	-0.46	-0.36	0.41
N:C					-0.34	0.19	**-0.89**	-0.19	-0.14	-0.09
N:N						-0.41	0.02	-0.63	-0.18	0.30
O:H_N							0.14	-0.10	-0.13	-0.18
O:C								0.41	0.32	-0.22
O:N									0.62	-0.32
O:O										-0.19

H_N:H_N	-0.56	0.38	-0.30	-0.31	-0.47	0.02	-0.42	-0.02	0.66	-0.15
C:H_N	0.46	-0.56	0.38	-0.30	-0.31	-0.47	0.02	-0.42	-0.02	0.66
C:C	-0.42	0.11	-0.53	0.46	0.56	0.56	-0.64	0.02	0.46	-0.50
N:H_N	0.18	-0.24	0.00	0.31	0.10	0.21	**-0.96**	-0.40	0.59	-0.01
N:C	0.22	-0.02	0.24	0.15	0.07	-0.63	-0.23	**-0.90**	0.67	-0.24
N:N	-0.59	-0.14	**-0.73**	0.03	**0.72**	0.64	-0.41	0.28	0.31	-0.15
O:H_N	-0.21	0.67	0.04	-0.22	-0.24	-0.35	0.33	0.07	0.13	-0.28
O:C	-0.22	0.17	-0.14	-0.27	-0.25	0.28	0.58	**0.86**	**-0.80**	0.26
O:N	0.55	-0.43	0.56	-0.41	-0.49	-0.47	0.64	0.03	-0.70	0.68
O:O	-0.19	-0.32	-0.20	-0.22	-0.34	-0.32	0.45	0.20	-0.56	**0.77**
Cl:H_N	-0.13	-0.10	-0.17	-0.02	0.17	0.56	-0.46	0.14	0.28	0.07
Cl:C		-0.41	**0.96**	-0.16	-0.26	-0.43	0.01	-0.52	-0.05	0.16
Cl:N			-0.22	0.51	-0.34	0.15	-0.01	0.35	-0.03	-0.65
Cl:O				-0.19	-0.35	-0.51	0.15	-0.47	-0.09	0.07
Cl:Cl					-0.29	0.29	-0.43	0.04	-0.04	-0.52
H_C:H_N						0.23	-0.10	-0.21	0.57	-0.29
H_C:C							-0.34	0.65	-0.09	-0.19
H_C:N								0.24	-0.59	0.19
H_C:O									-0.64	0.12
H_C:Cl										-0.40
***c*(E,E')**	**Cl:C**	**Cl:N**	**Cl:O**	**Cl:Cl**	**H_C:H_N**	**H_C:C**	**H_C:N**	**H_C:O**	**H_C:Cl**	**H_C:H_C**

Figure S13

Scatterplot of H_N…N distance *vs*. lattice electrostatic energy in the **Clxx** crystal structures with one molecule per asymmetric unit. **Clpo_O** was excluded due to absence of any H_N…N hydrogen bonding interaction.

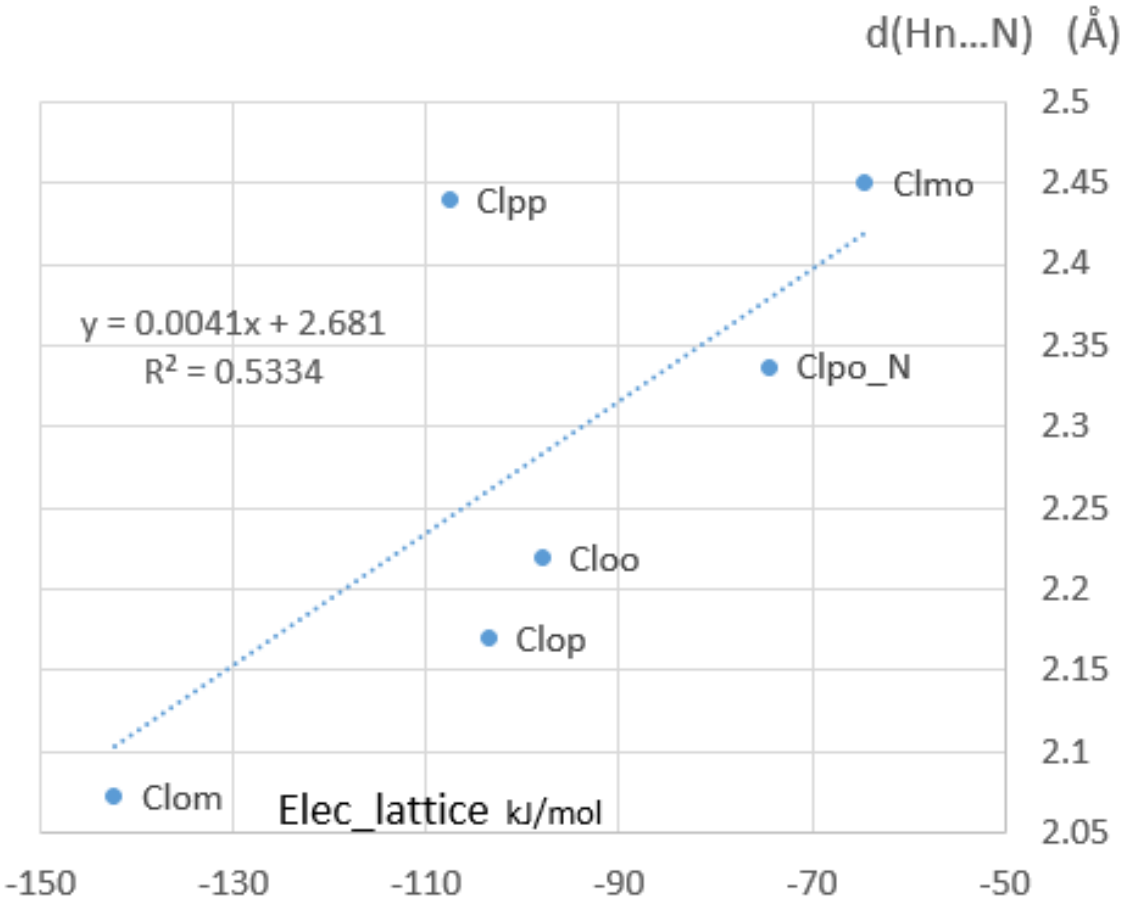

Figure S14

(*a*) Deformation of the transferred electron density in the **Clom** dimer (inversion center) in the C-Cl…Cl-C plane. Contour +/- 0.05 e/Å^3.

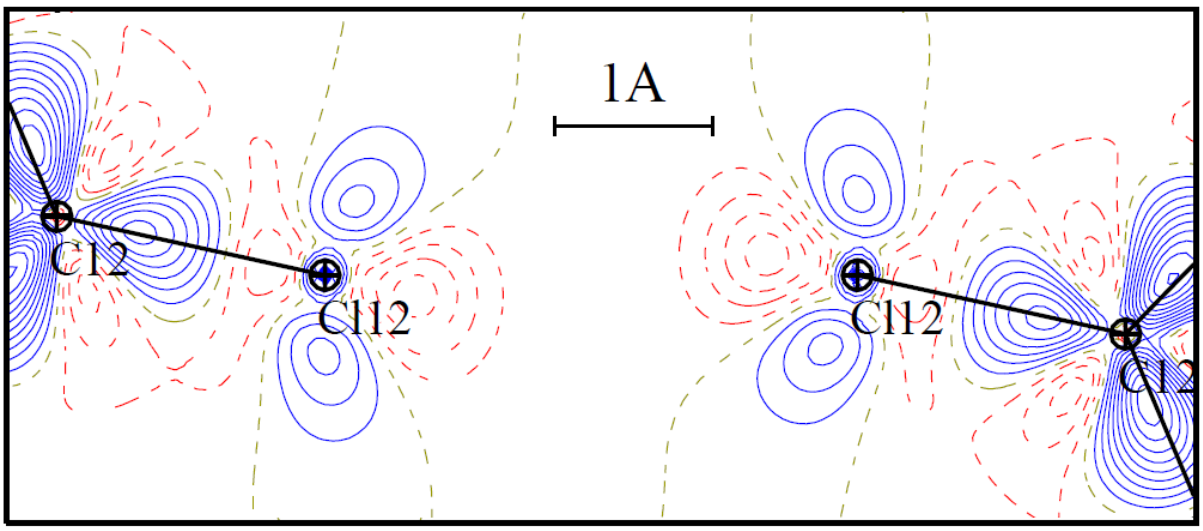

(*b*) Electrostatic potential generated by each chlorine atom alone.

Contours +/- 0.02 e/Å. **Green** and **blue**: positive; purple and **red**: negative, grey and yellow: zero contour.

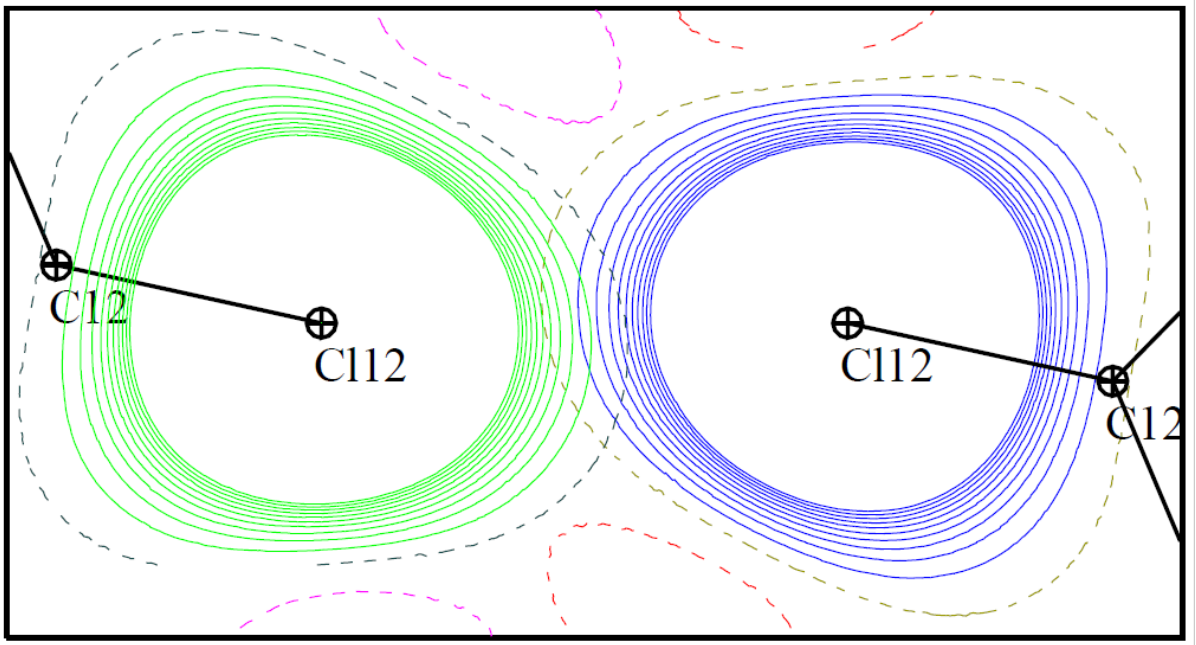

See **Results and Discussion** section in main manuscript:
Ab initio modelling and conformational analyses section (last couple of paragraphs).